SANDIA REPORT

SAND2013-3459
Unlimited Release
Printed June 2013

Photovoltaic Ground Fault and Blind Spot Electrical Simulations

Jack D. Flicker
Jay Johnson

Prepared by
Sandia National Laboratories
Albuquerque, New Mexico 87185 and Livermore, California 94550

Sandia National Laboratories is a multi-program laboratory managed and operated by Sandia Corporation, a wholly owned subsidiary of Lockheed Martin Corporation, for the U.S. Department of Energy's National Nuclear Security Administration under contract DE-AC04-94AL85000.

Issued by Sandia National Laboratories, operated for the United States Department of Energy by Sandia Corporation.

Available to DOE and DOE contractors from
U.S. Department of Energy
Office of Scientific and Technical Information
P.O. Box 62
Oak Ridge, TN 37831

Telephone: (865) 576-8401
Facsimile: (865) 576-5728
E-Mail: reports@adonis.osti.gov
Online ordering: http://www.osti.gov/bridge

Available to the public from
U.S. Department of Commerce
National Technical Information Service
5285 Port Royal Rd.
Springfield, VA 22161

Telephone: (800) 553-6847
Facsimile: (703) 605-6900
E-Mail: orders@ntis.fedworld.gov
Online order: http://www.ntis.gov/help/ordermethods.asp?loc=7-4-0#online

SAND2013-3459
Unlimited Release
Printed June 2013

Photovoltaic Ground Fault and Blind Spot Electrical Simulations

Jack D. Flicker
Jay Johnson
Photovoltaic and Distributed Systems Integration
Sandia National Laboratories
P.O. Box 5800
Albuquerque, New Mexico 87185-MS1033

Abstract

Ground faults in photovoltaic (PV) systems pose a fire and shock hazard. To mitigate these risks, AC-isolated, DC grounded PV systems in the United States use Ground Fault Protection Devices (GFPDs), e.g., fuses, to de-energize the PV system when there is a ground fault. Recently the effectiveness of these protection devices has come under question because multiple fires have started when ground faults went undetected. In order to understand the limitations of fuse-based ground fault protection in PV systems, analytical and numerical simulations of different ground faults were performed. The numerical simulations were conducted with Simulation Program with Integrated Circuit Emphasis (SPICE) using a circuit model of the PV system which included the modules, wiring, switchgear, grounded or ungrounded components, and the inverter. The derivation of the SPICE model and the results of parametric fault current studies are provided with varying array topologies, fuse sizes, and fault impedances. Closed-form analytical approximations for GFPD currents from faults to the grounded current carrying conductor—known as "blind spot" ground faults—are derived to provide greater understanding of the influence of array impedances on fault currents. The behavior of the array during various ground faults is studied for a range of ground fault fuse sizes to determine if reducing the size of the fuse improves ground fault detection sensitivity. The results of the simulations show that reducing the amperage rating of the protective fuse does increase fault current detection sensitivity without increasing the likelihood of nuisance trips to a degree. Unfortunately, this benefit reaches a limit as fuses become smaller and their internal resistance increases to the point of becoming a major element in the fault current circuit.

ACKNOWLEDGMENTS

The authors would like to acknowledge the Solar America Board for Codes and Standards (Solar ABCs) Blind Spot Ground Fault Working Group for valuable direction and periodic reviews of this work.

Contents

FIGURES

TABLES

NOMENCLATURE

A	Ampere
AC	Alternating Current
AWG	American Wire Gauge
CCC	Current Carrying Conductor
c-Si	Crystalline Silicon
DC	Direct Current
EGC	Equipment Grounding Conductor
GFDI	Ground Fault Detector Interrupter
GFPD	Ground Fault Protection Device
G_{min}	SPICE minimum conductance
IEC	International Electrotechnical Commission
I_{fault}	Current through ground fault
I_{GFPD}	Current through GFPD
I_{leak}	Module Leakage Current
I_{leak}^{string}	Module leakage per string
I_{mp}	Current at Maximum Power
I_{OCPD}	Current through OCPD
I_{sat}	Module Diode Leakage Current
I_{sc}	Module Short-Circuit Current
I_{shunt}	SPICE current through device shunt
IV	Current Voltage
KCL	Kirchoff's Current Law
kcmil	Circular mil
KVL	Kirchoff's Voltage Law
kW	Kilowatt
M	Number of modules per string
MPPT	Maximum Power Point Tracking
NEC	National Electrical Code
OCPD	Overcurrent Protection Device
P_{mp}	Power at Maximum Point
R_{comb}	Resistance of combiner cabling
R_{EGC}	Resistance of EGC
RF	Radio Frequency
R_{fault}	Ground Fault Resistance
R_{GFPD}	Resistance of GFPD
R_{leak}	Leakage Current Resistance
R_{max}^{trip}	Maximum detectable fault resistance
R_{mp}	Inverter Impedance at Maximum Power
R_{PV}	Resistance of PV cabling
R_{recomb}	Recombiner Cable Resistance
R_s	Module Series Resistance
R_{sh}	Module Shunt Resistance
R_{shunt}	SPICE instrinsice shunt resistance
R_x	Resistance of portion of PV cabling included in fault loop
S	Number of parallel strings in array

SPICE	Simulation Program with Circuit Emphasis
UL	Underwriters' Laboratory
V	Voltage
V_{mp}	Voltage at Maximum Power
V_{oc}	Open Circuit Voltage

This page is intentionally left blank.

1. INTRODUCTION

The mechanical, electrical, or chemical degradation of photovoltaic systems can lead to a number of fault scenarios. In this report, we investigate the electrical behavior of PV systems that have undergone an electrical fault to ground from different locations in the PV array. Faults of different impedances are simulated on arrays of varying sizes to determine fault characteristics on residential, commercial, and utility scale systems. Recently, a "blind spot" in the traditional ground fault protective system has been identified for grounded and isolated PV systems which are the most common in the United States. This occurs in cases where there exists an undetected ground fault to the grounded current-carrying conductor, and then a second fault occurs in the array. At this point, the Ground Fault Protection Device (GFPD)—often called the Ground Fault Detector/Interrupter (GFDI)—is not capable of de-energizing the fault and multiple fires have resulted [1]. Industry leaders have suggested lowering the GFPD (e.g., fuse) ratings would improve the chances of detecting high impedance, low current ground faults. In order to better understand the impact of changing the fuse ratings on ground fault protection systems, a range of leakage current cases were simulated to quantify the likelihood of nuisance trips with reduced GFPD ratings. The simulations on different array sizes show that decreasing GFPD ratings improves the number of low-impedance faults that can be detected without increasing the number of nuisance trips to some extent. In the case of blind spot ground faults where there is a ground fault to the grounded current-carrying conductor, decreasing the fuse size below 1 A does not improve the number of detectable ground faults because the internal resistance of the fuse prevents the current from passing through the GFPD. Therefore, decreasing GFPD ratings alone will not mitigate all ground faults and alternative ground fault detecting tools are required to identify blind spot faults.

This page is intentionally left blank.

2. SPICE PV MODEL AND INVERTER MODEL CREATION

To simulate faults to different PV systems, PV arrays were constructed with multiple modules connected to a central inverter. While there are a number of PV configurations and topologies in the United States, the most common is the DC-grounded, AC-isolated system. Unfortunately this design is known to have problems with undetectable ground faults [1, 13]. As a result, the simulations focused on this topology to identify the depth and severity of the problem.

PV modules are non-linear circuits. Their behavior is difficult to describe analytically without transcendental equations, but the use of computer circuit simulations can describe the behavior of a PV system for a wide variety of fault conditions [2]. A common method of circuit simulation is the use of the Simulation Program with Integrated Circuit Emphasis (SPICE). SPICE, originally developed at the University of California, Berkeley Electronics Research Laboratory in 1973 [3], is a general-purpose, open source, analog circuit simulator used to predict circuit behavior. In this work, the program MacSPICE, a derivative of SPICE3f4, was used to analyze the behavior of PV systems in various array configurations and ground-fault conditions [4].

The SPICE model of the PV array is accomplished through the construction of a PV module using a one-diode model, as depicted in Figure 1. These modules consist of an ideal current source (I_{sc}) in parallel with a diode and shunt resistance (R_{sh}) and in series with a series resistance (R_s). In order to increase the V_{oc} of the module above the voltage drop of a regular diode (~0.6 V), the ideality constant of the diode is increased [5].

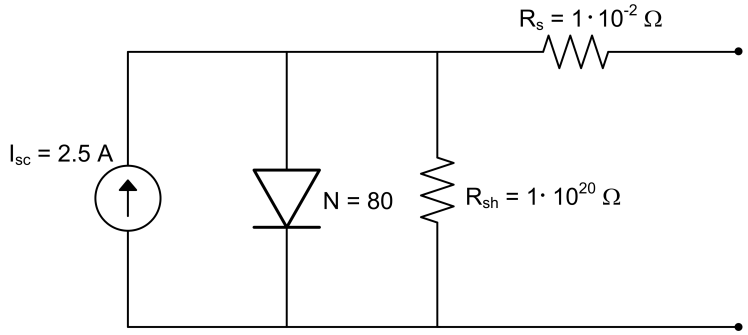

Figure 1: One diode model for single PV module.

This one diode model allows for total customization of the module IV curve. The slope of the IV curve around V_{oc} is controlled by the value of R_{sh}. The slope of the IV curve around I_{sc} is controlled by the value of R_s. The value of the current source determines the value of I_{sc}, while the diode ideality constant, N, determines the V_{oc}, shown in Figure 2.

For the purposes of this work, the one-diode model is constructed to approximate a nearly perfect photovoltaic module. The current source is set to supply 2.5 A at short circuit, the diode has an ideality factor of N=80, the shunt resistance is set $1 \cdot 10^{20}\ \Omega$ and the series resistance is set to 10 mΩ. This module gives an IV curve (green trace in Figure 2) with I_{sc} of 2.5 A, V_{oc} of 56 V, and P_{mp} of 118 W. The max power point has a current of I_{mp}=2.4 A and a voltage of V_{mp}=49.2 V.

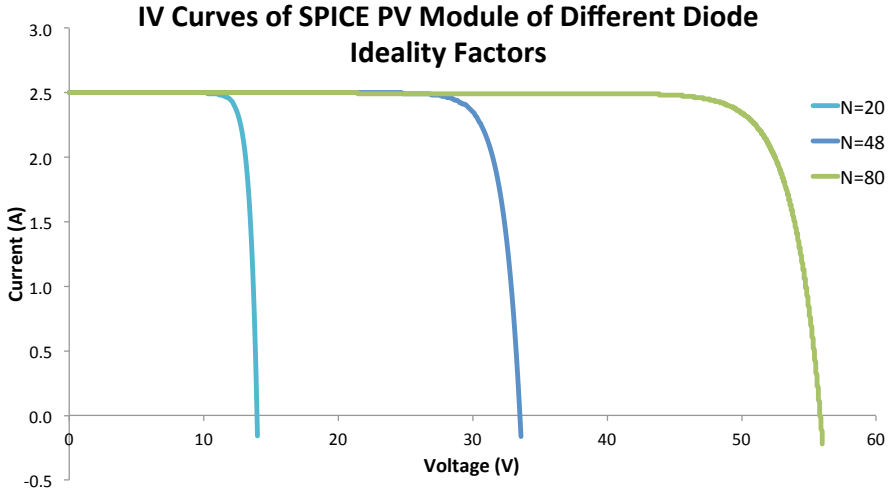

Figure 2: IV curves for one-diode PV module as diode ideality factor, N, is varied.

2.1. SPICE PV Array and Inverter Model Development

To determine the behavior of residential PV arrays during a ground fault, a model was created composed of a number of strings wired in parallel. Each string is composed of seven modules in series (Figure 4). Each module is connected to a bypass diode (I_{sat}=4.7·10^{-12} A, N=1). The array is wired to a resistor, as a basic approximation of the real input impedance of an inverter. The resistance connected to the array in all the simulations is set at the resistance required to generate maximum PV power, R_{mp}, of the unfaulted array.

2.2. Inverter Model Simplifications

As stated earlier, a DC-grounded, AC-isolated central inverter is modeled in each of the simulations because this topology is susceptible to faults that are undetected by the ground fault fuse. Only the real component of the inverter impedance is modeled, although physical inverters are a complex system containing transistors, capacitors, and switching controls [6]. However, if the voltage ripple and max power tracking [7] are ignored, the PV system can be approximated by a steady state DC system with a constant resistance. This means that the imaginary components of the inverter impedance have no effect on the steady state solution before and after the fault occurrence. This may not necessarily be the case during the transient time period when the fault occurs; there is a discrete change in system state, in which the storage elements in the inverter backfeed current through the PV system if there are no blocking diodes [8, 9]. As will be shown later, the inverter bus capacitor is charged to V_{mp} before the fault, but the ground fault drops the operating voltage of the array so the capacitor discharges into the array. This spike in current into the array is large, but the time period of the backfeed is unlikely to trip a GFPD fuse. If, for example, a 2-string array with a 1 mF capacitor is considered (a common capacitance to have in a residential inverter), the time required for the fault current transient to drop below the trip level of a 1 A would be on the order of 15 ms (59 J of dissipated energy), shown in Figure 3.

The Littelfuse KLKD 1 A fuse, a common "midget" style fuse used in residential inverters, requires 30 ms to clear at a current of 5 A (210 J) [10]. This does not take into account the resistance of the fuse, which will decrease the magnitude of the voltage spike. Thus, a real fuse will have a smaller current spike and is unlikely to trip during such a fault event.

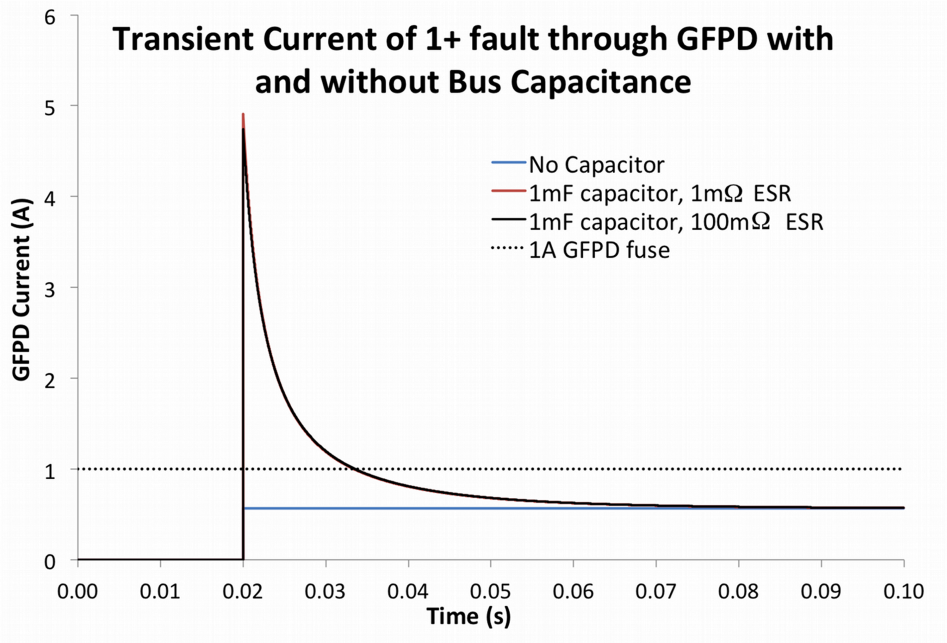

Figure 3: Transient GFPD current of a 1+ fault with and without connection to an inverter bus capacitor. The blue trace shows the transient GFPD current with the inverter modeled only as a resistive element. The overlapped red and black traces show the inverter modeled as a complex impedance with a 1 mF bus capacitor and a capacitor series resistance of 1 mΩ (red) and 100 mΩ (black).

Larger inverters tend to have higher capacitance values and correspondingly higher fuse trip points. The increase in capacitance increases the amount of stored energy available to trip the GFPD. This energy will be released more slowly by altering the RC time constant of the capacitor discharge, causing the GFPD current to remain higher for longer. However, this is offset by three factors:

(1) In large inverters, the GFPD rating is increased so that more peak current for much longer time periods is required to trip the fuse. For example, in Figure 3, even for very large capacitance values (~10 mF), if the GFPD trip point is set at 3, 4, or 5 A, the fuse is unlikely to trip.

(2) As the fuse trip point increases, the intrinsic resistance of the fuse decreases and the ratio of power dissipated by the GFPD compared to the fault is lowered. So larger fuse sizes dissipate smaller percentage of the capacitor energy compared to lower fuse values and are less likely to trip due to the capacitor discharge.

(3) For a large number of strings, the voltage drop in the array due to a single faulted string is small, therefore, the energy supplied by the capacitor

(dependent on the difference in the square of the voltages) is small compared to a smaller array (which has a larger voltage drop due to a fault in a single string).

Based on these factors, it is unlikely that the imaginary components of the inverter impedance will affect GFPD fuse response and the inverter may be simplified to a resistive element. However, more advanced modeling of the inverter/PV system interaction does warrant future study.

2.3. Identification of fault locations

With this model of a PV system, various ground faults were modeled. The ground faults can occur inside modules, in conductors between modules, and in DC runs; however, due to the limitations of the SPICE model, faults within the module to the frame are not considered. Blind spot ground fault simulations are a more complicated situation requiring the modeling of the conductor impedances and are investigated in Section 6. In the SPICE array models, a fault to ground is composed of a controllable switch and a resistor. As a method of categorizing the location of the fault on the faulted string, the fault is named for the module and terminal that the fault originates. For example, the fault shown in Figure 4 would be labeled as 4+, since the fault occurs from ground to the positive terminal of module #4. It is to be noted that a ground fault at 4+ is synonymous with a fault at 5-. However, for consistency, the nomenclature will only refer to ground faults at the positive terminal of a module.

2.4. SPICE ground fault modeling details

The shunt resistance (R_{shunt}) around the ground fault switch is implicit in SPICE simulations and is present for any device that results in a sudden, discrete voltage change (e.g. switches, diodes). This is necessary in nodal analysis programs, such as SPICE, to prevent floating voltages that can lead to singular conduction matrices and unstable circuit simulations. This resistance is set to the reciprocal of the minimum conductance (G_{min}). For this series of simulations, G_{min} is set to $1 \cdot 10^{-10}$ resulting in a value for I_{shunt} in the range of nanoamperes. Due to this modeling limitation, no element ever has zero current flow, but will instead have some very small nonzero current dependent on the value of G_{min}.

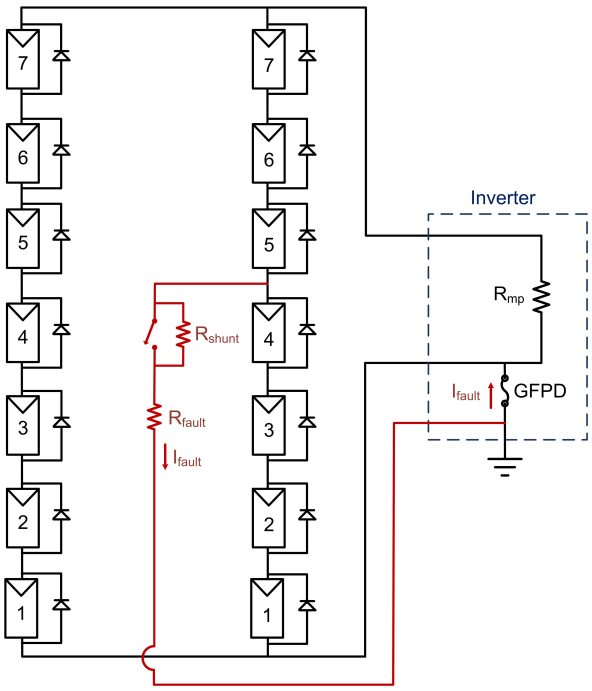

Figure 4: Schematic diagram of two-string PV array with seven modules per string. When the switch is closed String #2 is faulted to ground through a resistor, R_{fault}, at position 4+.

2.5. Equivalence of solid ground fault and arcing ground fault

Two distinct types of faults may occur from string to ground: the first is a fault in which two conductive elements make continuous physical contact and current flows between them. A simple resistance may easily model this type of fault. A second type of fault, known as an arc-fault, occurs when two exposed conductors at different electrical potentials approach or briefly contact each other. Rather than making firm contact, current flows via the electrical breakdown of gas between the two conductors without a physical connection between the two.

Previous work on DC arcs [11, 12] has shown that an arc is a highly nonlinear system, with a non-constant resistance. The current-voltage properties of DC arcs for systems with copper electrodes and an air gap between 1 and 10 mm were investigated by Nottington *et al.* and can be described by Eq. (1):

$$V = A + \frac{B}{I^n} \tag{1}$$

where A = 27.5, B = 44, and n = 0.67. A nonlinear resistor is most easily accomplished in SPICE using a current-controlled voltage source with a voltage value equal to Eq. (1). However, simulations show the non-linear resistance characteristics of the DC-arc have no impact on the transient characteristics of the faulted array. Figure 5 shows the similarity in transient behavior between a non-linear SPICE current-controlled voltage source (left) and a regular resistor in

series with a switch (right). Both transients act as a step function because the simulation is assumed to be ideal with no energy storing elements in the circuit.

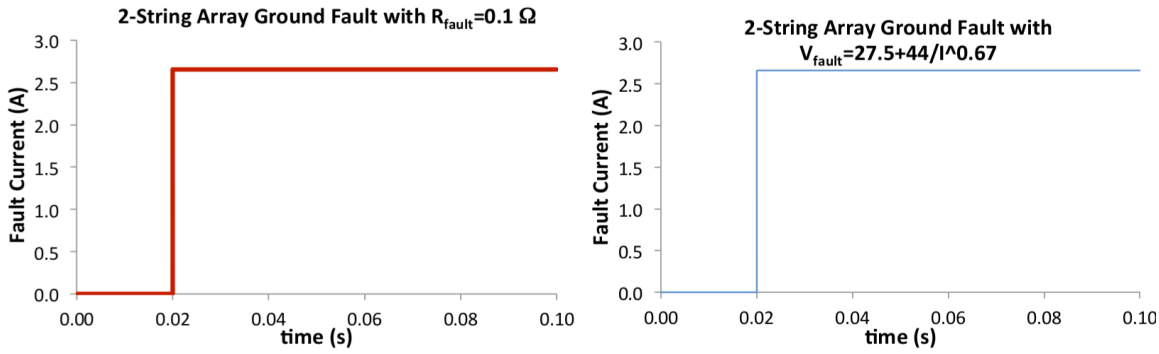

Figure 5: Fault current for a two-string array using both a non-linear current-controlled voltage source (left) and a simple linear resistor (right). The fault location for these simulations is 4+.

If inductive and capacitive parasitics, such as those present in real systems, are added to the circuit simulations, there will be greater variation between modeling the fault as a simple linear resistor compared to the non-linear DC arc model. Since there was no analytical difference in the transient effects of the non-linear and linear representations of the arc-fault resistance, a simple resistor in series with a switch was chosen to model the ground fault for both simple and arcing ground faults.

3. GROUND FAULTS IN TWO-STRING ARRAYS WITHOUT LEAKAGE CURRENTS

The first set of ground fault simulations were for a two-string array with string #2 faulted to ground. The value of R_{fault} was varied from 0.1 to $1 \cdot 10^{21}$ Ω at module nodes 1+ through 7+. In these simulations, none of the bypass diodes turned on and the only current flow through the diodes was consistent with leakage current due to G_{min}, on the order of nA.

3.1. Module performance with ground fault

The voltage output of the array decreased with decreasing fault resistance due to the presence of a fault. A fault at 4+ with R_{fault}=100 Ω, shown in Figure 6, decreased the applied voltage across each module in string #1 and moved the operating point of each module on string #1 toward short circuit (red circle on inset of Figure 6). The current output of string #1, therefore, increased compared to the unfaulted case.

The presence of a fault splits the modules of string #2 to different operating points. If, for example, the fault is located from 4+ to ground, as shown in Figure 6, the voltage at point 4+ is pulled down to a voltage of $V = I_{fault} \cdot R_{fault}$. The modules that are below the fault decrease in applied voltage, so that their operating point moves towards short circuit (blue circle in inset of Figure 6). Those modules source current close to I_{sc}. The modules above the fault have an applied voltage that is greater than in the unfaulted condition, causing their operating point to move towards V_{oc} (green circles in inset of Figure 6). These modules source less current than the unfaulted case. Through the use of Kirchoff's Current Law (KCL), the difference between the current sourced by the modules below the fault plus the fault current must equal to the current sourced by the modules above the fault. In addition to the fault current, which does not reach the inverter, the total output power of the array is significantly reduced during the fault, since all the modules are shifted off the maximum power point.

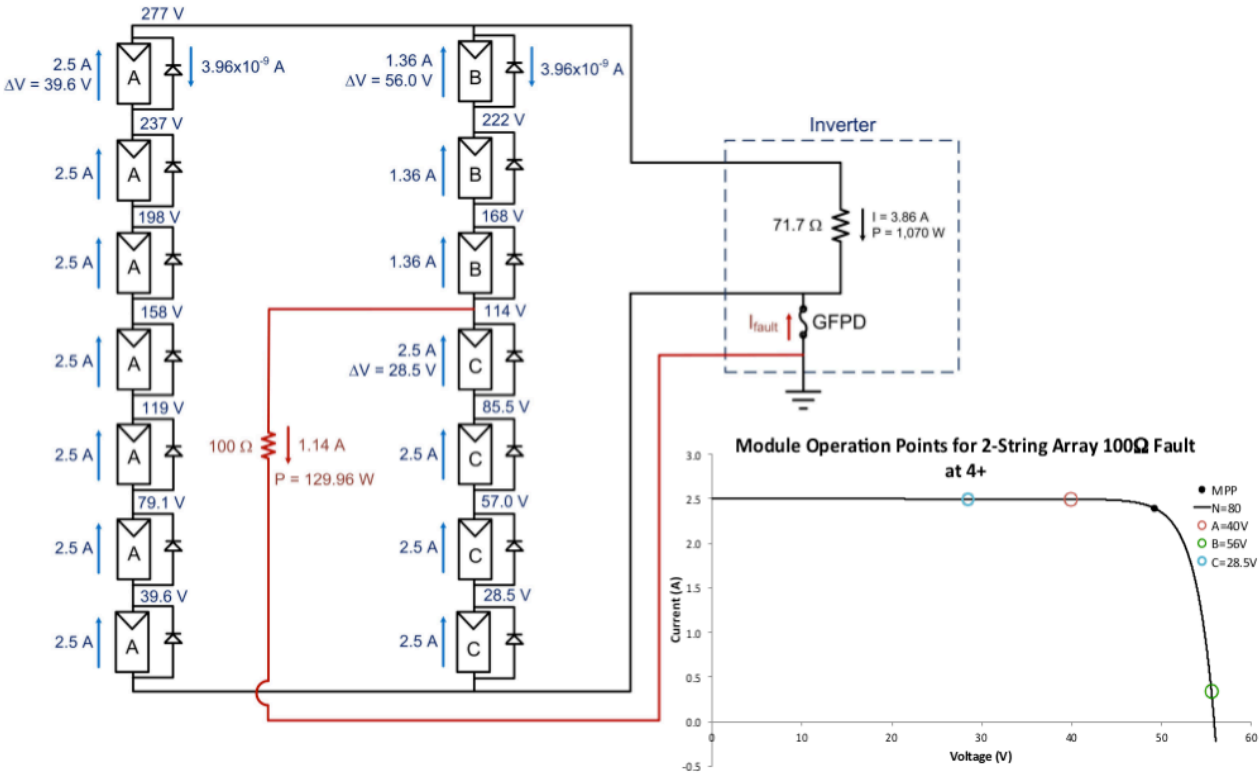

Figure 6: Example simulation results for a two-string array with a 100 Ω ground fault located at 4+ of string #2. Before, the fault, the operating point of the array is at maximum power (black dot in inset picture). After the fault, the applied voltage of the array decreases, so the operating voltage of the modules in string #1 decrease (labeled A), increasing the amount of current sourced. The applied voltage of modules below the fault on string #2 (labeled as C) show a decrease in applied voltage at operating point, while those modules above the fault (labeled B) show an increase in the voltage at operating point.

3.2. Ground fault resistance influence on GFPD fault detection

The effect of the ground fault on the array is dependent on both its location and resistance. The example fault in Figure 6 shows a relatively high resistance fault. This high resistance type of fault may occur due to corrosion or partial conductor insulation failure due to cracking, degradation, or breakdown.

Low resistance faults and faults incorporating more modules (e. g. at 7+) increase the power through the fault path and therefore increase the probability of a fire. The results of all the simulations (R_{fault}=0.1 to $1 \cdot 10^{21}$ Ω at 1+ to 7+) are shown in Figure 7. Figure A shows the behavior of the array voltage as a function of R_{fault} for locations 1+ to 7+ on string #2. The voltage of the array decreases sharply once the value of R_{fault} is below ~1000 Ω. Other than the value of R_{fault}, the array voltage is highly dependent on the location of the fault. The array voltage decreases more when the fault occurs closer to the positive end of the string.

Similar results can be seen for the array current (Figure 7 B) and array power (Figure 1 C). As expected, the current through R_{fault} has the opposite behavior (Figure 7 D); the value of I_{fault} increases dramatically for values of R_{fault} less than ~1000 Ω and as the number of faulted modules on string #2 increases. For R_{fault}=0.1 Ω, which would represent a reasonably solid fault connection, the dependence of I_{fault} on the number of faulted modules is linear (Figure 8). This indicates ground faults that incorporate fewer modules will be more difficult to detect, since less current flows through the fault and a higher sensitivity fuse must be used. For example, if a 1 A GFPD fuse (dashed line in Figure 8) was used for this two-string array, a ground fault with R_{fault}=0.1 Ω at 1+ would never trip the fuse since I_{fault} is only 0.568 A. In this case, the ground fault would remain indefinitely.

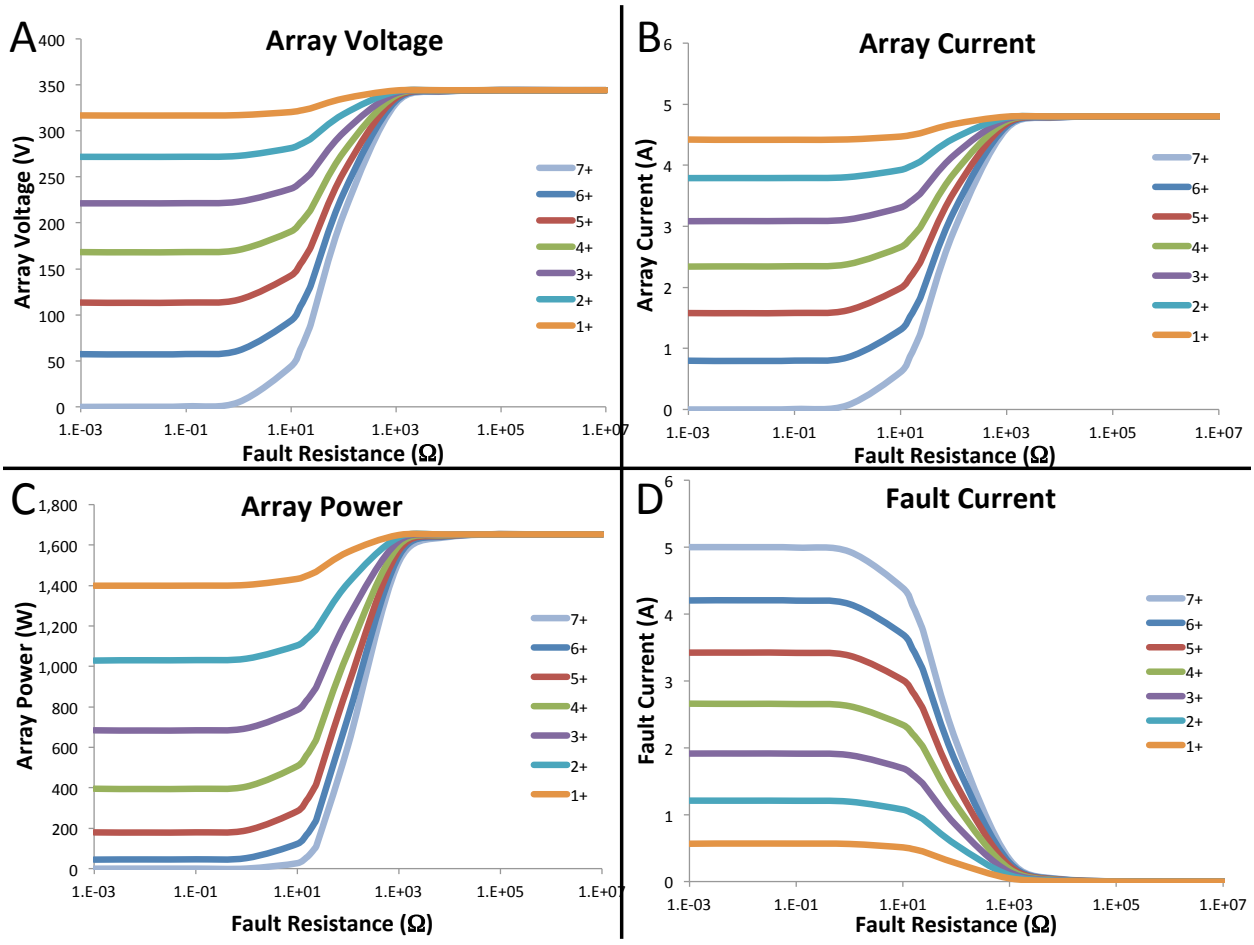

Figure 7: Results of ground fault SPICE simulations for a two-string array with a ground fault located on string #2 at various nodes (1+ through 7+). Quadrant A shows the array voltage as a function of fault resistance. The array voltage decreases dramatically as more modules are faulted and for fault resistance below ~1000 Ω. Similar results can be seen for array current (B) and output power (C). Quadrant D shows the fault current increases as the number of faulted modules increases and fault resistance decreases below ~1000 Ω.

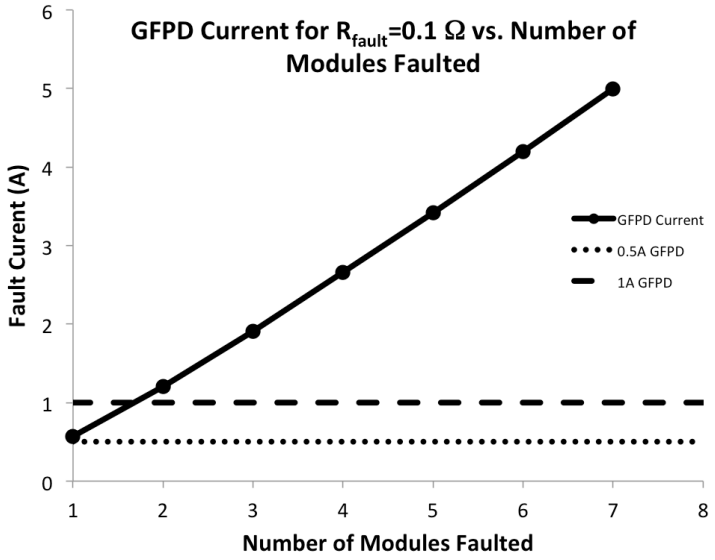

Figure 8: Graph of fault current vs. number of modules faulted for a fault resistance of 0.1 Ω. The fault current increases nearly linearly with the number of faulted modules.

3.3. GFPD current dependence on irradiance

The majority of circuit analyses and simulations assume that the PV array operates at 100% solar irradiance level or 1000 W/m^2. Unfortunately, in the field, arrays are only at this irradiance level for a short period of time. Reduced irradiance level means that modules source less current and less current flows through the GFPD, making faults harder to detect. It is also possible for the irradiance to exceed 1000 W/m^2 depending on the altitude of the installation, atmospheric aerosols, and cloud enhancement, so in those cases there would be more current through the fault path and the ground fault would be easier to detect. Figure 9 shows the IV curves and module operation points for a 100 Ω fault at 4+ of a two-string array at various irradiance levels. The MPP of the array is indicated by the colored point. The operation point of modules in the unfaulted string (A) is denoted by the black squares. Modules above the fault (B) are represented by the black 'x' while modules below the fault (C) are indicated by the black circles.

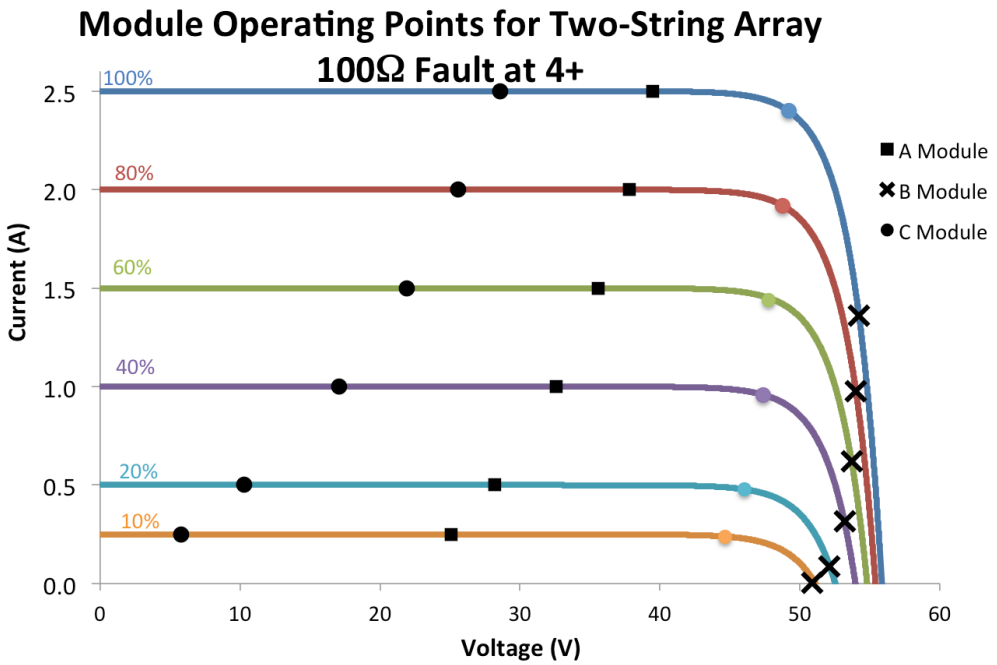

Figure 9: Module IV curves and module operating points for a 100 Ω ground fault at 4+ for a two-string array at various irradiance levels. The MPP is denoted by the colored dot. The module labels are the same as used in Figure 6. "A" modules are in the unfaulted string, "B" modules are above the fault, and "C" modules are below the fault.

For PV modules at the MPP, the current sourced can be approximated as a linear function of the irradiance while voltage output remains nearly constant. Due to this, as the irradiance level is decreased, the value of R_{mp} increases. This change in R_{mp} changes the behavior of GFPD current with respect to irradiance level. For small fault resistances, the GFPD current is linear with respect to irradiance level since $R_{fault} << R_{mp}$ for all irradiance levels (Figure 10, left). For larger values of R_{fault}, as irradiance level increases, the fault resistance becomes an appreciable fraction of R_{mp} and the GFPD current has a sub-linear dependence on the irradiance level. For large values of R_{fault}, $R_{fault} > R_{mp}$ for nearly all irradiance levels and most of the current flows through the load. In this case, GFPD current is nearly constant with regards to irradiance level. However, for all fault resistance values, the GFPD current is nearly linear with respect to the number of modules faulted (Figure 10, right). The slope of the linear relationship is dependent on the irradiance level. The largest slope corresponds to 100% irradiance (due to the increased module current at high irradiance values) with decreasing slope as the irradiance level decreases. Therefore, lower levels of irradiance yield lower GFPD currents.

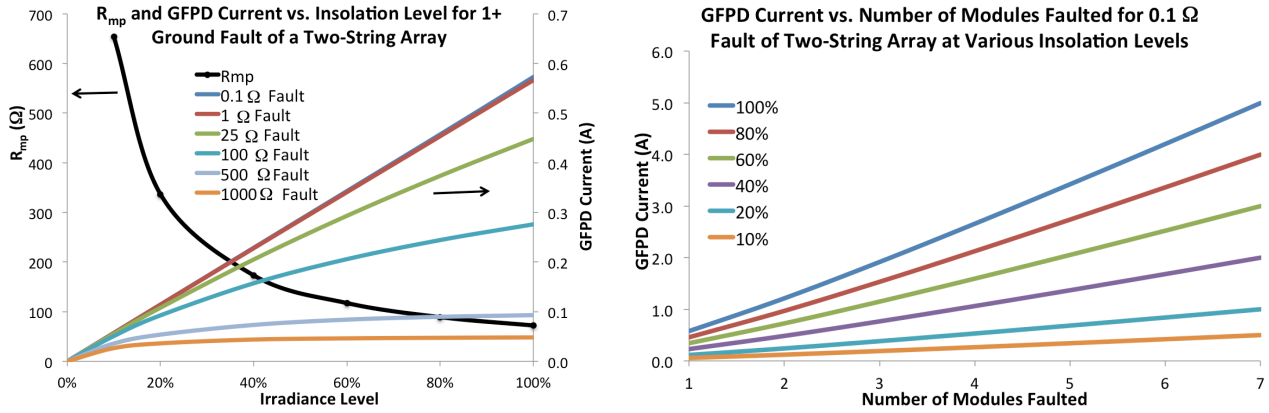

Figure 10: (left) GFPD Current vs. irradiance level for 1+ ground faults of various resistances. Array Rmp is denoted by the black trace. Low resistance faults are linear with respect to irradiance level while high resistance faults are sub-linear. (right) GFPD current vs. number of modules faulted for a 0.1 Ω fault. The GFPD current is linear for all irradiance levels, though lower irradiance levels yield lower GFPD current. The linear trend holds for higher impedance faults.

3.4. Backfed currents in faulted string

It was mentioned previously that the modules on string #2 located above the fault have an increased voltage compared to the unfaulted case. For sufficiently low resistances, the fault is effectively at ground potential and the entire array voltage is applied to these modules, moving them towards V_{oc}.

If the fault is composed of enough modules and the fault resistance is low, it is possible for the modules above the fault on string #2 to be biased at voltages equal to or greater than V_{oc}. This means that those modules back-feed current from the unfaulted strings through the ground fault. Figure 11 shows the current from faulted string #2 as a function of fault resistance. For resistances below ~1000 Ω, the sourced current decreases. For faults at 4+, 5+, and 6+, at low values of fault resistance, the sourced current from string #2 crosses the zero axis and inverts. This indicates current backfeeds through the modules above the fault on string #2 to the fault so they no longer act as current sources, but as current sinks.

Figure 12 shows a schematic of a two-string array with a ground fault at 4+ such that the current sourced by string #2 is approximately zero. In this case (corresponding to R_{fault}=4.66 Ω), the modules above the fault are biased at V_{oc} and all the current sourced by modules below the fault runs through the fault. For values of R_{fault}<4.66 Ω, the current through the fault will increase above 2.5 A. In this case, the current though the inverter will fall below 2.5 A and the modules on string #2 above the fault will back-feed current from string #1 to the fault. For lower fault resistances, these modules will be biased above V_{oc} and will source current directly into the fault.

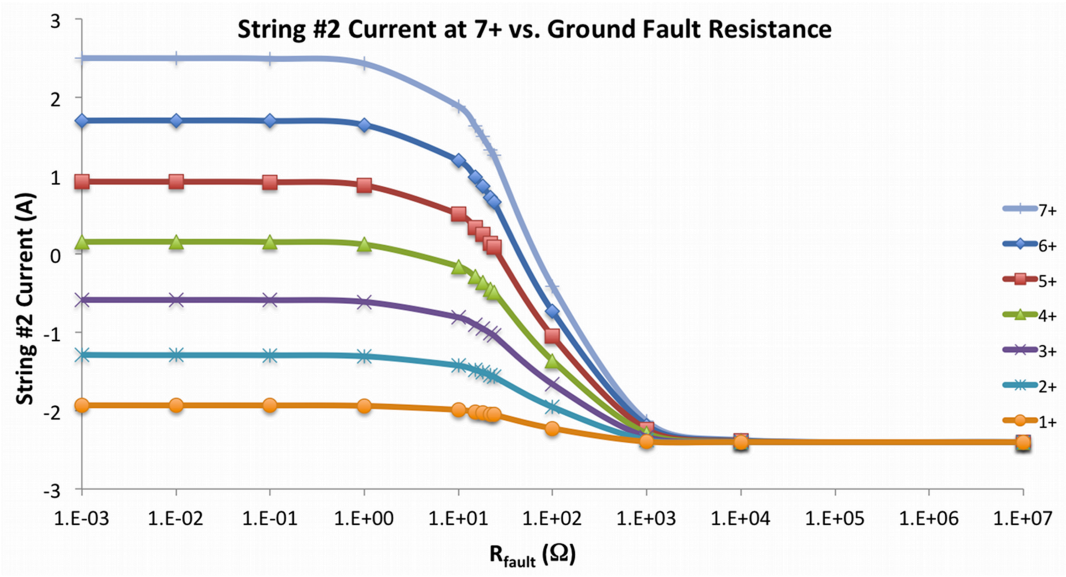

Figure 11: Graph of current from string #2 at 7+ in a two-string array as a function of fault resistance. The current sourced by string #2 decreases as the value of R_{fault} decreases below ~1000 Ω.

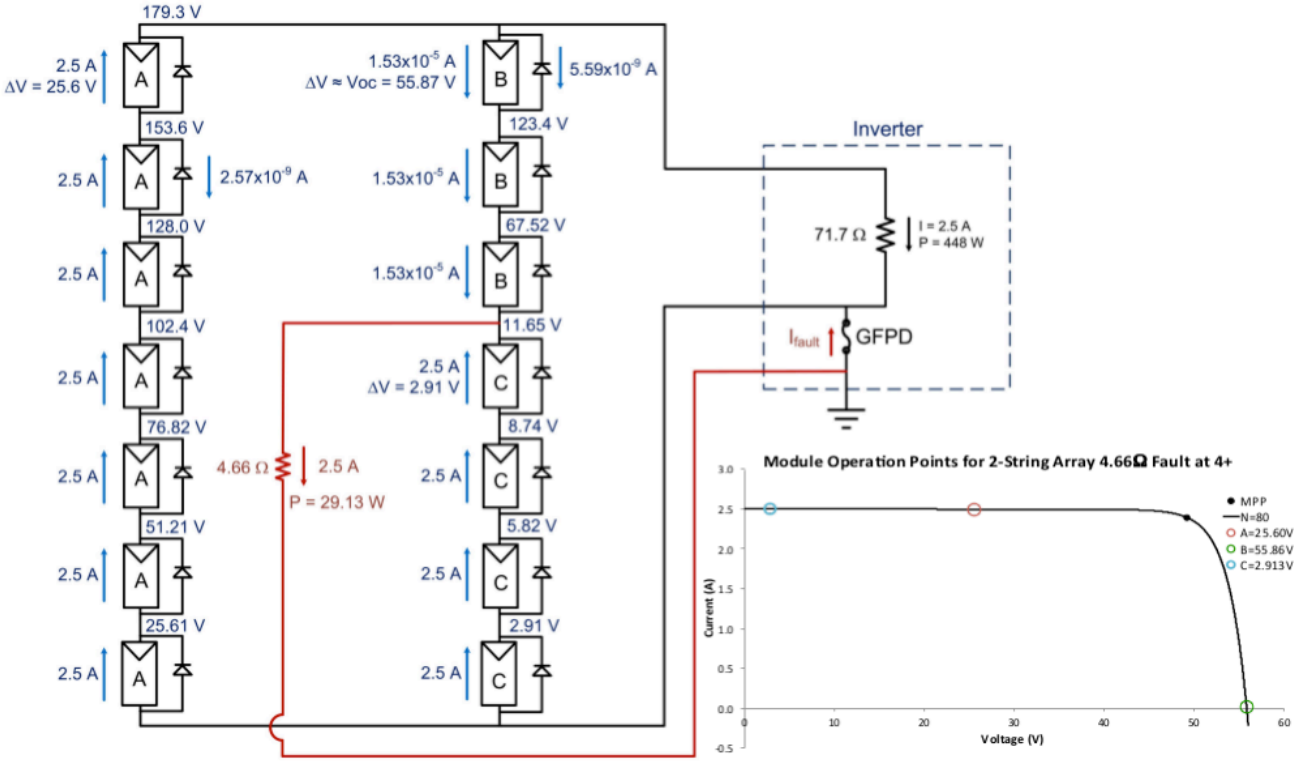

Figure 12: Schematic of a two-string array with a ground fault of 4.66 Ω located at 4+ of string #2. For this position and this fault resistance, the three modules above the fault must support nearly the entire string #1 voltage. This applies a voltage equal to V_{oc} of these modules, resulting in zero current generation. Inset shows the module IV curve and the operating points of the modules on string #1 (A, red dot), above the fault on string #2 (B, green dot) and below the fault on string #2 (C, blue dot).

This page is intentionally left blank.

4. GROUND FAULT PROTECTION VS. NUISANCE TRIPPING FOR ARRAYS WITH UP TO 10 STRINGS

When designing protection mechanisms for ground faults, the effect of leakage current on GFPD current is of primary importance. By simulating the leakage current, fuse ratings can be selected to more adequately protect against ground faults while mitigating nuisance trips. In this set of simulations, the ground fault behavior of two-, three-, and 10-string arrays with leakage currents were simulated. By including leakage currents, the risk of GFPD nuisance trips was investigated for various fuse ratings. These simulations model the ground fault fuse (GFPD) as an ideal fuse, (e.g. no internal resistance). In Section 5.7, the internal fuse resistance is included to better characterize system performance during a fault for different fuse ratings. Also, note that in real arrays, there are transient effects on the GFPD due to inverter operation, noise from the AC side, and RF effects on the array [13]. These current spikes are relatively short in duration, so they do not cause the fuse to clear, but they could account for nuisance trips if the current is close to the fuse rating. This effect is not included in these simulations.

4.1. Module leakage definition and modeling values

While there is current leakage from a number of places in the array, the primary source of leakage is in the modules. Module leakage current is defined as the current between the module, biased at some high voltage, and the grounded frame. Leakage current measurements are described by IEC 61215 (section 10.15.3) [14] and UL 1703 (section 21.5) [15]. For determining leakage current of a module, as described by UL 1703, both terminals of the module are at 500 V while the frame is held at ground. The leakage current is then defined as:

$$I_{leak} = \frac{V_{applied}}{R_{leak}} = \frac{500V}{R_{leak}} \tag{2}$$

For the purposes of the SPICE simulations, a variety of module leakage resistance values were chosen because these values change due to ambient conditions (rain, due, humidity, etc.), module technology, and age. The resistance values and their corresponding leakage currents (at an applied voltage of 500 V) are listed in Table 1. However, it should be noted that for the array used in the simulation (unfaulted array $V_{oc} \approx 395$ V), the applied voltage is less than 500 V for all modules, so the simulated leakage current from each module is given in the last two columns of Table 1 for modules 1 and 7.

Table 1: Values of module leakage resistance and corresponding leakage current chosen for different simulations. Green indicates the leakage is IEC 61215 compliant.

R_{leak} (MΩ)	I_{leak} @500 V (mA)	I_{leak} for Module 7 @V_{mp} (mA)	I_{leak} for Module 1 @V_{mp} (mA)
500	0.001	0.00069	0.000246
50	0.01	0.0069	0.00246
10	0.05	0.0344	0.0049
5	0.1	0.069	0.0246
0.5	1	0.69	0.246

In order to pass IEC 61215 standards, the measured R_{leak} of a crystalline silicon module must be greater than 40 MΩ·m^2. For typical module sizes (1.12-1.5 m^2), this would give a maximum module leakage current of 14-18.75 μA. The values of R_{leak} shown in Table 1 accurately capture both the leakage of pristine, new modules and the added leakage which might occur due to voltage or humidity stress in the field.

The leakage current values in Table 1 were chosen in order to both capture the variety of leakage measurements taken from modules in the field and overestimate the leakage of modules to create a safety factor for fuse trip setting recommendations. This is necessary because module leakage in fielded units can vary many orders of magnitude. Module leakages ranging from values of ~100 nA to 100 μA were extensively measured by del Cueto *et al.* [16]. Values of leakage currents for different fielded arrays are presented in the Solar ABCs paper, "Final Report: Examination of Inverter Ground-Fault Detection 'Blind Spot' with Recommendations for Mitigation" [13].

4.2. SPICE leakage model

When multiple modules are placed in series to form a string, the frames of all the modules are connected to earth via equipment grounding conductors [17]. This results in the circuit schematic of an array with leakage as shown in Figure 13. The positive terminal of each module in a string has a leakage resistor connected to ground. The current leakage from any single module in an array may be described by:

$$I_{leak}^{\text{module}} = \frac{V}{R_{leak}} \tag{3}$$

Since the resistance of R_{leak} is modeled as the same value for each module, the leakage current will be greatest for modules at the top of the string with the highest voltage to ground, shown in Table 1.

The module voltage above ground increases with the number of modules in a string. In an unfaulted array, each module is at an electrical potential V_{mp} higher above ground than the module below it. Therefore, the module leakage per string (I_{leak}^{string}) is dependent on the number of modules in the string, M, by:

$$I_{leak}^{string} = \sum_{i=1}^{M} \frac{i \cdot V_{mp}}{R_{leak}} \tag{4}$$

For the 7-module strings used in these simulations (V_{mp} = 49.2 V), the maximum IEC allowable leakage current per string (R_{leak} = 40 MΩ·m^2) for a 1.5 m^2 module would be 51.66 μA/string.

In order to increase array efficiency, there is a trend towards creating higher voltage arrays in "behind the fence" utility-scale installations where the 600 V *National Electrical Code®* (*NEC*) 690.7 limits do not apply. An array operating at 600 V would be composed of approximate 10 SPICE PV modules, yielding a maximum IEC leakage of 101.48 μA/string (1.96x increase). An array at 1000 V would be composed of around 18 PV modules, yielding a maximum IEC leakage of 315.5 μA/string (6.08x increase).

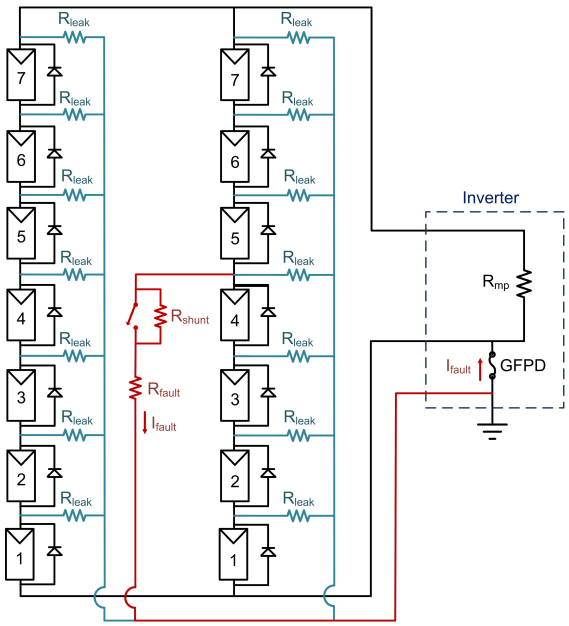

Figure 13: Schematic for an array of modules that have a leakage current, R_{leak}.

4.3. Module leakage influence on ground fault simulations

In order to determine the effect of module leakage current on GFPD current, simulations for ground faults at 1+, 4+, and 7+ in two-, three-, and 10-string arrays were performed using R_{leak} values from Table 1. Figure 14 shows the results for these simulations.

Figure 14A shows the fault current as a function of fault resistance for a two-string array with a module leakage of 1 μA (at 500 V). The results are very similar to the simulations without module leakage. The dashed line indicates where a 1 A fuse would trip. The dotted line

indicates the trip point for a 0.1 A fuse. It is interesting to note that for this array, the 1+ fault current (green) never reaches 1 A, so a fuse of this size would never trip. For a given fault, there is a general increase in the maximum trip resistance (R_{max}^{trip}) as the number of strings increases, though the effect is sub-linear. Additional discussion of the maximum trip resistances are presented in section 5.2

Figure 14B and C show similar data for three- and 10-string arrays with 1 μA of leakage current for each module. This indicates that ground faults in arrays with larger string sizes would be easier to detect due to the higher current through the fault. The higher currents are from the other strings backfeeding through the fault path. Figure 14D shows the results of a ground fault at 1+ for a 10-string array for module leakage values from 1 μA to 1 mA. For most fault resistances the leakage current has little effect on the GFPD current, so the lines cannot be resolved. At very low values of R_{fault}, there is a slight dependence of leakage current on GFPD current.

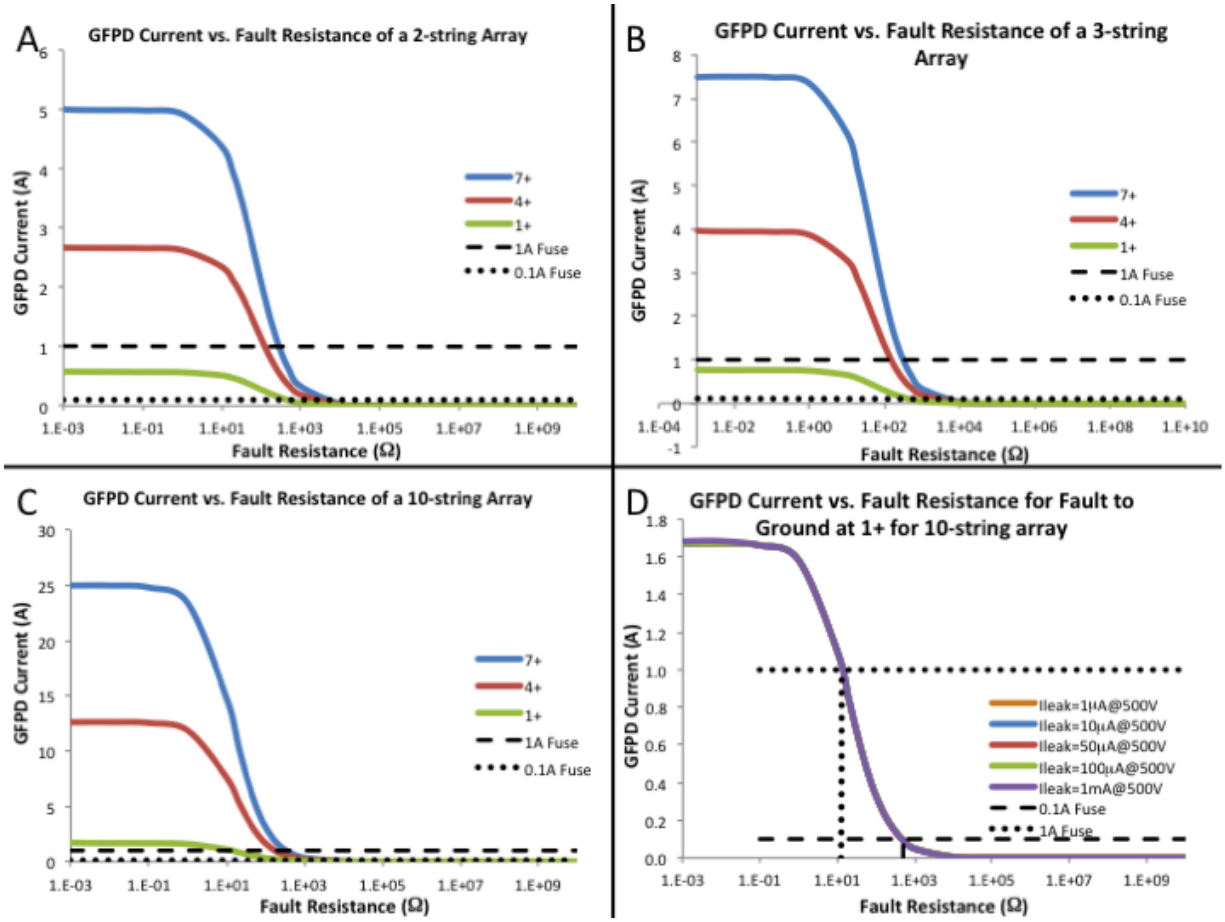

Figure 14: Fault current vs. fault resistance for a ground fault at 1+, 4+, and 7+ for a (A) 2-string, (B) 3-string, and (C) 10-string array with 1 μA of module leakage. (D) shows a ground fault at 1+ of a 10-string array for a wide variety of module leakage values. There is little difference in the fault current for different values of module leakage.

There is almost no GFPD current dependence on module leakage. Figure 15 shows the relationship between GFPD current and module leakage current for all simulations (ground faults at 1+, 4+, and 7+ of two-, three-, and 10-string arrays). The value of the GFPD current only depends on the location of the fault and the number of strings in the array. The fault current increases as the number of faulted modules or number of strings in the array increase. The value of I_{GFPD} seems to scale linearly with the number of strings. If the data is normalized by the number of strings in the array, then the fault current depends principally on the location of the fault.

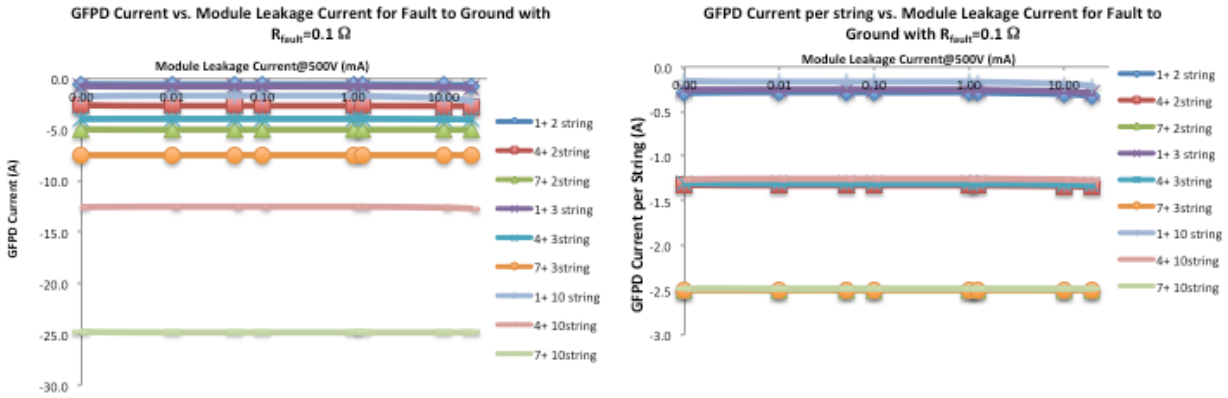

Figure 15: (left) Graph of fault current as a function of module leakage for ground faults at 1+, 4+, and 7+ in 2-, 3-, and 10-string arrays. There is little dependence on the fault current with module leakage. The fault current is a function of fault placement and number of strings. (Right) Graph of fault current as a function of module leakage normalized for number of strings in the array. If the fault current is normalized by the number of strings, the fault current is only a function of the location of the fault.

This page is intentionally left blank.

5. GROUND FAULT PROTECTION VS. NUISANCE TRIPPING FOR ARRAYS WITH MORE THAN 10 STRINGS

The simulation of high power arrays is important since utility-scale systems pose the greatest ground fault fire hazard because of the increased number of failure points (e.g., connectors) and the higher operating currents. In order to characterize the maximum fault resistance that can be detected by the GFPD, or R_{trip}^{max}, as a function of string size, a set of simulations were carried out for larger arrays.

5.1. SPICE large array model creation

To make these large arrays computationally feasible, the simulation structure of the PV array was slightly changed. For small (<10 strings) array sizes, the sub-circuit building block for the array is the PV module, as described earlier. For array sizes larger than 10 strings, a new sub-circuit was constructed. This new sub-circuit building block is composed of 10 parallel strings, each string with 7 modules in series. While this larger sub-circuit makes large-scale arrays more computationally manageable, it sacrifices some of the granularity present in small-scale simulations. For example, if the sub-circuit building block of the array is a block of 10 strings, it is not possible to find applied voltage and current sourced from individual modules inside the sub-circuit.

Simulations were carried out for arrays composed of one- through 201-strings of 7 modules each with ground faults at 1+, 4+, and 7+ on one string. Each module was simulated with a value of I_{leak}=1 μA at an applied voltage of 500 V ($R_{leak}=5 \cdot 10^{-8}$ Ω). As in previous simulation sets, the load resistance is set at R_{mp} for the array. In this set of simulations, in order to find how R_{trip}^{max} varies as a function of the number of strings in the array for a 0.1 A and 1 A fuse, the value of R_{fault} was varied until I_{GFPD} was equal to 0.1 or 1 A. A 0.1 A fuse will trip for any value of R_{fault} lower than R_{trip}^{max} (i.e., if I_{GFPD}>0.1 A).

5.2. Detectable and undetectable faults to ground

The results of the simulations for a 0.1 A fuse are shown in Figure 16. The value of R_{trip}^{max} for a 0.1 A fuse with a fault at 1+ is indicated by diamonds. The area below this line is colored in dark gray to indicate that smaller R_{fault} values will blow a 0.1 A fuse. Resistances above this line do not carry enough current to blow the fuse. Similar results are shown for faults at 4+ (squares, with $R_{fault}<R_{trip}^{max}$ in medium dark gray) and 7+ (triangles, with $R<R_{trip}^{max}$ in light gray). Similar results are shown for a 1 A fuse in Figure 17.

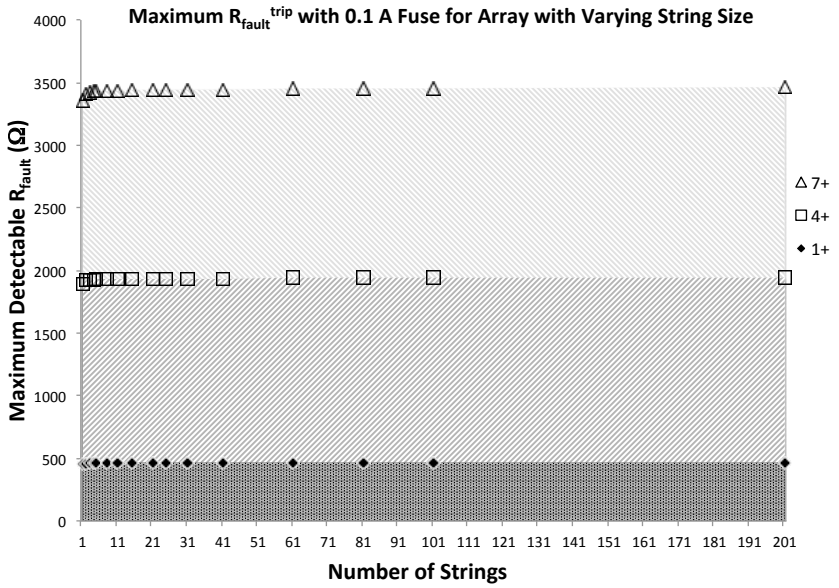

Figure 16: R_{trip}^{max} as a function of array size with a 0.1 A fuse for faults at 1+, 4+, and 7+. Diamonds indicate R_{trip}^{max} for a 0.1 A fuse with a fault at 1+. Detectable fault resistances ($R_{fault}<R_{trip}^{max}$) are colored in dark gray. Squares indicate R_{trip}^{max} for a fault at 4+ with detectable resistances colored in medium dark gray. R_{trip}^{max} for a fault at 7+ is indicated by triangles and all detectable resistances are colored light gray.

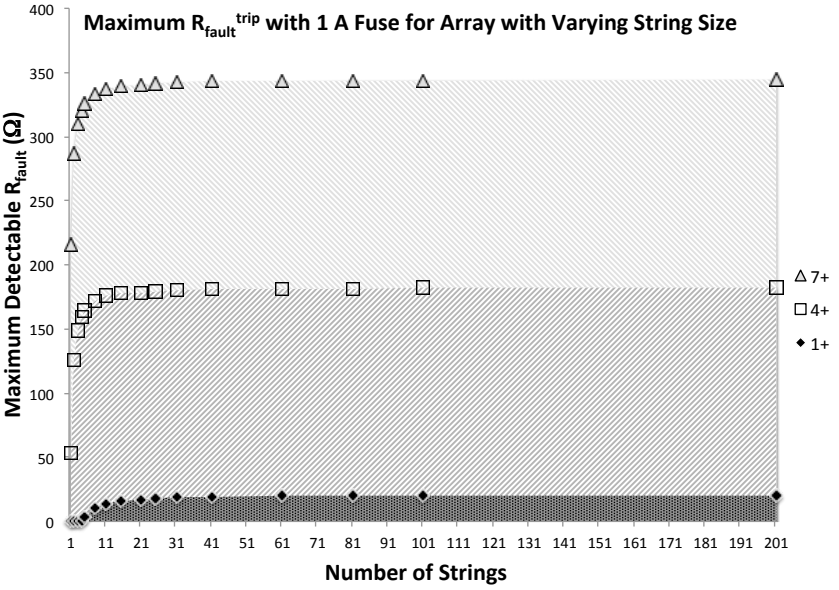

Figure 17: R_{trip}^{max} as a function of array size with a 1 A fuse for faults at 1+, 4+, and 7+. Diamonds indicate R_{trip}^{max} for a 1 A fuse with a fault at 1+. Detectable fault resistances ($R_{fault}<R_{trip}^{max}$) are colored in dark gray. Squares indicate R_{trip}^{max} for a fault at 4+ with detectable resistances colored in medium dark gray. R_{trip}^{max} for a fault at 7+ is indicated by triangles and all detectable resistances are colored light gray.

In arrays with more than ~20 strings, the detectable fault resistances for 1 A fuses are approximately $1/10^{th}$ as large as 0.1 A fuses. This means that the 0.1 A fuse is more capable of detecting high impedance faults. The second trend to be noted from Figure 16 and Figure 17 is that while ground faults less than ~1000 Ω tend to divert significant amounts of power from the load (Figure 7C); they may not all necessarily be detectable through fusing. For example, a 1 A fuse would be unable to detect a 500 Ω fault, regardless of the fault position or the number of strings. Such a fault would go undetected, sapping power from the inverter for long periods of time. For a 0.1 A fuse, only a 1000 Ω fault at 1+ would go undetected, but would be readily detected at 4+ and 7+ for all array sizes.

Another interesting trend is the value of R_{trip}^{max} increases rapidly for arrays with a small (<10) number of strings before leveling out for higher (>10) number of strings. This effect is due to the changing effective resistance, R_{mp}, of the inverter as the number of strings increase. There is little dependence of array size on I_{GFPD} for large array sizes because the R_{mp} value remains relatively constant for larger array sizes. In fact, the only dependence that array size has on R_{trip}^{max} is a slight increase due to increased module leakage current. For this array configuration with a leakage current of 1 μA (at a 500 V module bias) per module, this only yields an additional GFPD current of 2.75 μA per added string. Such a small additional current will not substantially affect R_{trip}^{max}, even for large array sizes.

5.3. Array size effect on detectable ground faults

The fact that R_{trip}^{max} (and therefore I_{GFPD}) is independent of array size for arrays larger than 10 strings indicates that the ability to detect faults does not become easier as strings are added onto an array. The fact that R_{trip}^{max} is nearly linear with respect to array size for small arrays and independent of array size is a result of the changing R_{mp}. Array R_{mp} is a ratio of array voltage to array current, shown in Eq. (5):

$$R_{mp}^{array} = \frac{V_{mp}^{array}}{I_{mp}^{array}} = \frac{M \cdot V_{mp}^{\text{module}}}{S \cdot I_{mp}^{\text{module}}} = \frac{M}{S} R_{mp}^{\text{module}} \tag{5}$$

where, S is the number of strings in parallel and M is the number of modules per string. As more strings are added to the array, array current increases while array voltage stays constant; this decreases the value of R_{mp}, as shown in Figure 18. Thus, as array size increases and R_{mp} decreases, more current is diverted away from the fault and flows through the load instead. This means that a greater percentage of power flows through the load compared to the fault for large arrays, so a ground fault is less detrimental. However, it also means that ground faults are harder to detect. However, note that increasing the string size increases R_{mp} and faults are more easily detected through fusing.

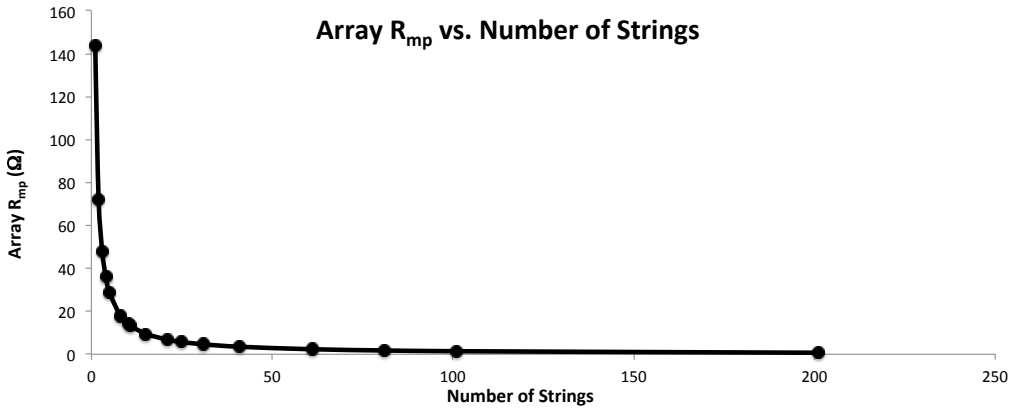

Figure 18: If array size is increased by added strings in parallel, the array R_{mp} falls as 1/N, where N is the number of strings. This lower R_{mp} causes a higher percentage of array current to flow through the ground fault.

5.4. Module leakage effects on detectable ground faults

In order to investigate the effects of leakage current on I_{GFPD} and R_{trip}^{max}, arrays composed of two- through 201-strings were simulated with module leakage currents from 1 μA to 1 mA per module (at 500 V bias). The results for a fault at 4+ with a 1 A fuse are shown in Figure 19. It can be seen that the value of R_{trip}^{max} for all traces has an inverse relationship to R_{mp} (black trace). The dependence of R_{trip}^{max} on array size also varies considerably with module leakage due to the addition of module leakage current to the fault current through the GFPD.

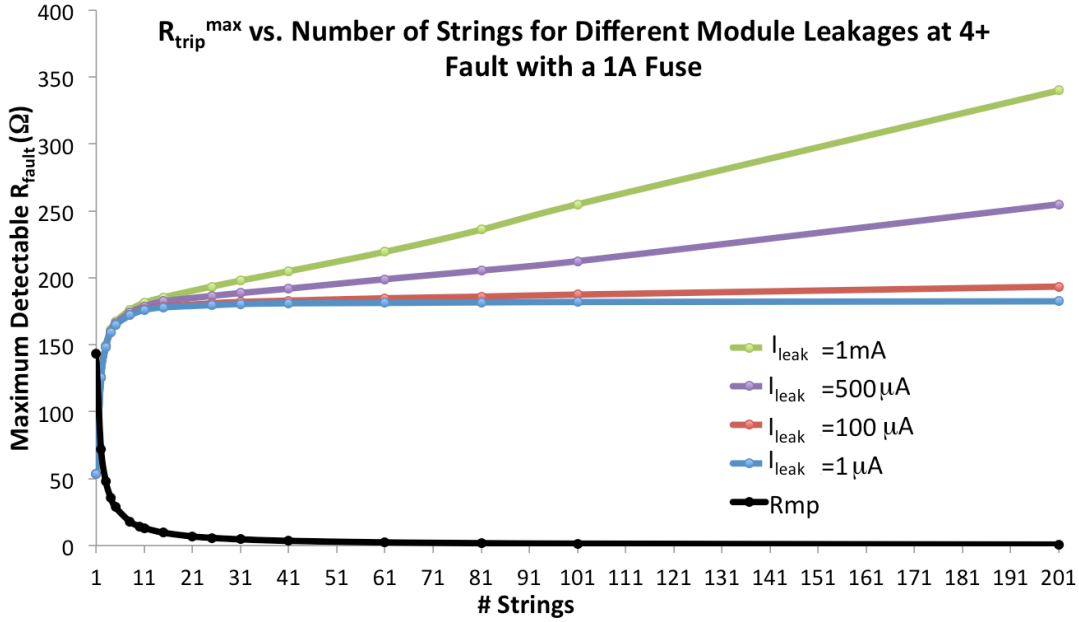

Figure 19: R_{trip}^{max} vs. array size for a 1 A fuse with a fault at 4+ and different modules leakages. In general, the R_{trip}^{max}, and therefore, the I_{GFPD} is inversely proportional to the load resistance (R_{mp}) which leads to the different behavior of R_{trip}^{max} vs. array size for small and large arrays. It can be seen that R_{trip}^{max} increases with increasing module leakage and array size.

However, it is common to increase GFPD ratings in larger inverters to mitigate nuisance trips from leakage currents. Figure 20 shows a graph of GFPD ratings vs. inverter power capability for a number of inverter manufacturers. GFPD ratings are typically 1 A for inverters smaller than 10 kW, 2 or 3 A for 10 to 100 kW, and 4 or 5 A for sizes greater than 100 kW. Also plotted on the graph is the IEC mandated maximum module leakage (40 MΩ·m^2 for a 1.5m^2 module) as a function of inverter power assuming the string parameters as discussed in section 2.1. For this array configuration, the maximum module leakage current is only 28.5 mA for a 491 kW array. For all inverter sizes, the leakage current is well below 1 A.

The array configuration used in this simulation is of lower voltage (345 V) than typically used in the most PV installations (~500 V depending on local ambient temperatures). The boost in voltage resulting from a greater number of modules per string will increase the leakage current through the GFPD. However, if the number of modules per string is increased to 10 in order to more accurately describe a real system in extremely cold conditions, the leakage current only increases by a factor of 1.94. This means that for a system at 600 V, the maximum leakage current would be 50.7 mA for a 491 kW array. Even this increased leakage current is well below the trip point of the lowest power inverters and indicates that, regardless of inverter size, GFPD trip point can be set at 1 A with little risk of nuisance tripping due to leakage current.

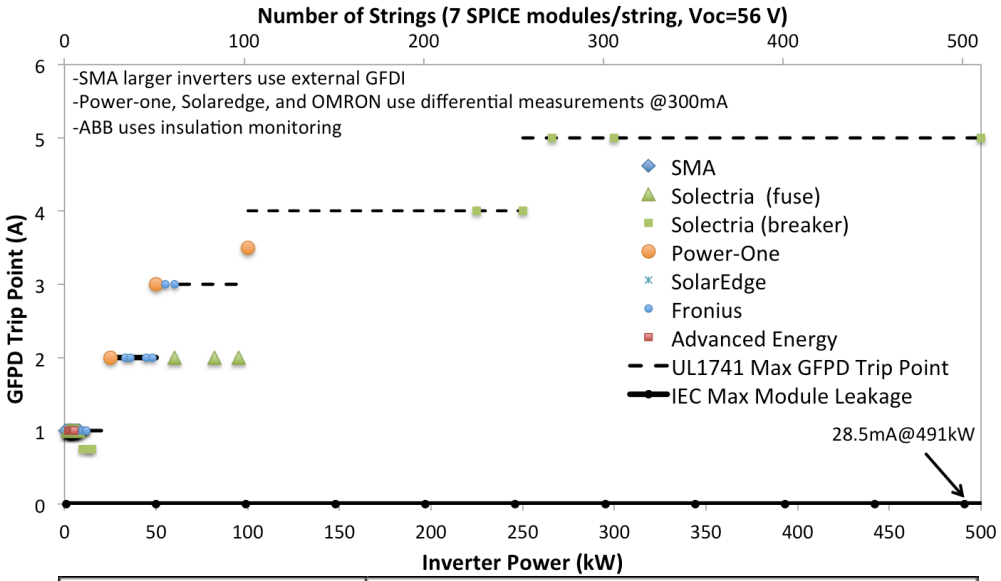

Device DC Rating (kW)	Max. Ground-Fault Current Detecting Setting (A)
0-25	1
25-50	2
50-100	3
100-250	4
>250	5

Figure 20: (top) Plot of GFPD trip point vs. rated inverter power for a number of commercially available inverters. As the inverter power increases, the GFPD trip point also increases. However, the maximum IEC allowable leakage current (black trace) is well below the GFPD trip points. (bottom) UL 1741 maximum allowable ground fault trip ranges are also displayed as a function of inverter DC power rating [18].

Figure 21 shows the results of GFPD fuse size on R_{trip}^{max}. Array sizes of one- through 25-strings (0.98 to 24.5kW) are shown with a 1 A fuse. Arrays sizes of 11- through 101-strings (10.8 to 99 kW) were simulated with a 2 A fuse. A 3 A fuse was used in the simulation of arrays from 61- to 301-strings (59.8 to 295 kW), while a 5 A fuse was used in simulation of arrays from 101- to 301 strings (99 to 295 kW).

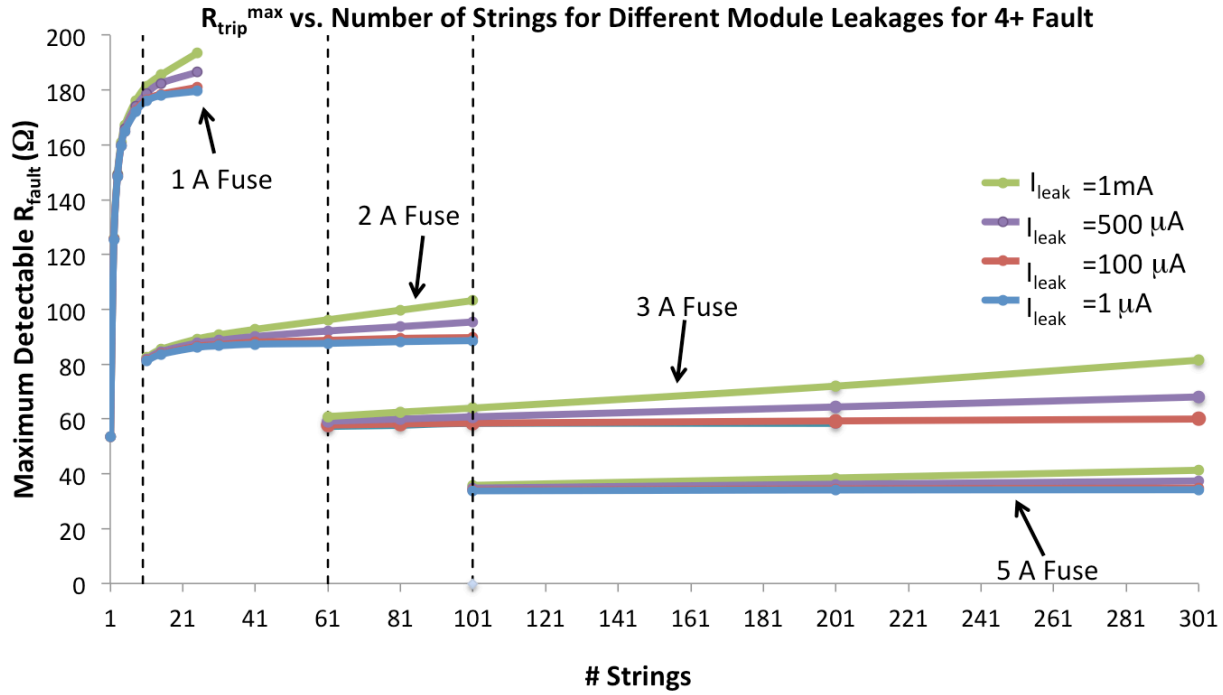

Figure 21: R_{trip}^{max} vs. array size for fault at 4+ with different fuse ratings and module leakages. As fuse rating is increased, the range of detectable fault resistances decreases. This indicates a greater probability of undetectable, high-impedance ground faults.

As shown above, the value of R_{trip}^{max} decreases as fuse ratings increases, since a much higher current is needed in order to trip the fuse. It should also be noted that module leakage has a much larger effect on R_{trip}^{max} for a 1 A fuse than for higher fuse ratings. Figure 22 (left) shows the dependence of R_{trip}^{max} for a 1, 5, and 10 A fuse on module leakage for a 101-string array. The percent change in R_{trip}^{max} as module leakage is changed from 1 μA to 1 mA per module decreases from 40.1% at a fuse rating of 1 A to just 3.1% at an oversized fuse rating of 10 A. Nuisance tripping due to leakage current is mitigated through the use of higher fuse ratings; however, this comes at the cost of decreased ground fault detection sensitivity.

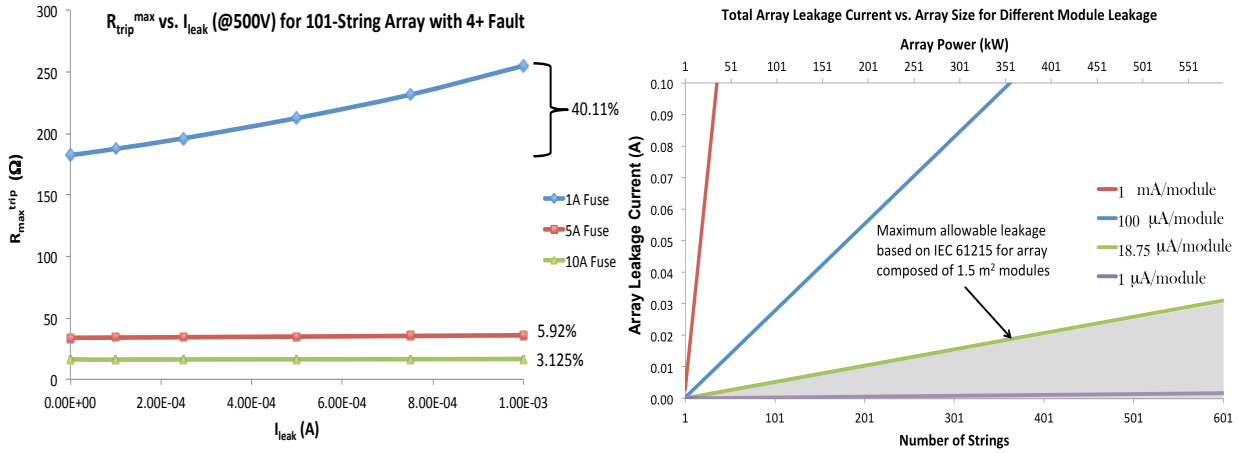

Figure 22: (left) R_{trip}^{max} vs leakage current per module for a 1 A, 5 A, and 10 A fuse. As the fuse rating increases, the percent change in R_{trip}^{max} due to leakage current decreases. (right) Total array leakage current vs. array size for module leakage (at 500 V applied bias) ranging from 1 µA to 1 mA.

5.5. Undetected faults due to large GFPD ratings

In order to determine optimal fuse sizing for a number of array sizes, simulations were carried out for faults of constant resistance varying the fault position and array sizes. The first set of simulations was completed for a 0.01 Ω fault at positions 1+ through 7+ with a module leakage rating of 100 µA/module (Figure 23, left). As can be seen, the GFPD current varies nearly linearly with regards to array size. The GFPD current is dependent on array size, even for large arrays because R_{fault} is small compared to R_{mp}.

For the majority of these faults, the current through the GFPD is so large that any fuse rating would protect against ground faults. However, the fault at 1+ shows much lower GFPD current (Figure 23, right). The 1+ fault line is sub-linear with a GFPD current and remains below 5 A. Two separate, nearly overlapping traces can be seen denoted by 1+. The green trace is I_{GFPD} without any module leakage while the green trace shows the effect of 100 µA module leakage. In order to fully protect a PV system from a fault of this type a 0.25 A fuse is needed for a single-string array (I_{GFPD}=0.34 A). A 0.5 A fuse would be sufficient for arrays from two- to five-strings (I_{GFPD}=0.572 to 1.08 A). For larger arrays, a 1 A fuse is needed, since the I_{GFPD} current does not reach 5 A, even for very large array systems. The 1 A fuse trip is well below the leakage level of 100 µA/module (blue trace), which would be approximately 0.165 A for a 500 kW system. Nuisance trips may be a problem for large leakage currents. A "worst case" leakage of 1 mA/module (53.3 times the IEC 61215 requirement), shown with the red trace, approaches 1 A for a 300 kW system so, in that case, it may be necessary to move to a larger fuse rating. Note that in this section the resistance of the GFPD is not considered in the simulations, but it is in Section 5.7.

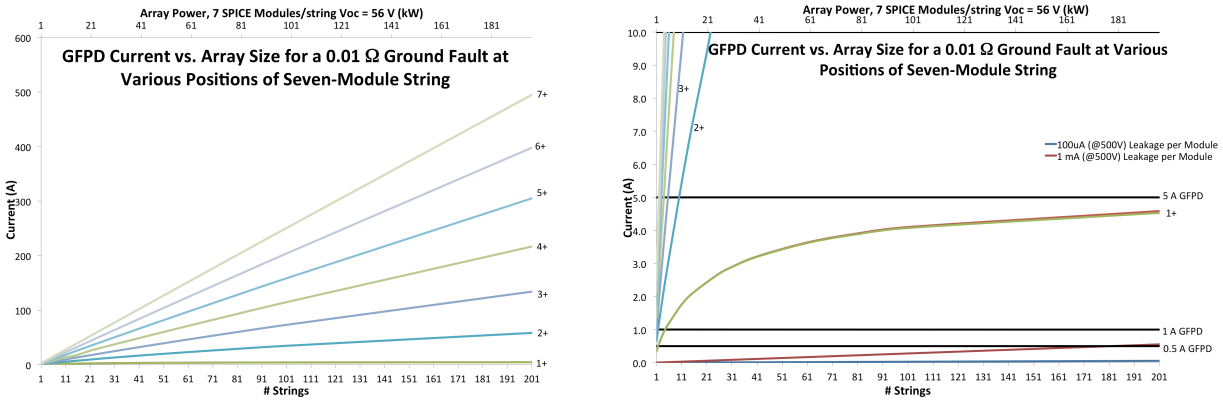

Figure 23: (left) GFPD current vs. array size for 0.01 Ω ground faults at various positions. The GFPD current is nearly linear with respect to array size due to the small fault resistance. (right) Close-up view of the 2+ and 1+ fault positions. The 1+ fault position has a sub-linear dependence on array size with little difference between modules exhibiting no leakage (green trace) with those exhibiting a "nominal" leakage currents of 100 μA/module (red trace). For array sizes above eight strings, a 1 A fuse would catch such a fault, but nuisance tripping may occur for high leakage rates, such as 1 mA/module (red trace) for arrays with more than 150 strings. Increasing the fuse rating to 5 A is not be sufficiently low to trip during a 0.01 Ω fault.

Another set of simulations was carried out for a 1 Ω fault at positions 1+ through 7+ with module leakages of 100 μA/module (Figure 24, left). The GFPD current is slightly sub-linear for faults at these resistances. This is due to the increased fault resistance. For large array sizes, the fault resistance is now an appreciable percentage of load resistance; so, as the number of strings increases, the percentage of current through the GFPD stays more constant than for the 0.01 Ω case.

Again, the discussion of this fault case will focus on the 1+ fault, since protection against this fault includes protection against the other fault positions—excluding "blind spot" faults discussed in Section 6. Figure 24 (right) shows a blown-up view of the 2+ and 1+ faults. The 1+ fuse current (green denotes no leakage while red denotes 100 μA/module leakage) for the 1 Ω case is smaller GFPD current compared to the 0.01 Ω case. The curve levels out at high string numbers around 4 A. To fully protect a PV system from a 1 Ω fault, it would be recommended to have a 0.25 A fuse for one-string array (I_{GFPD}=0.34 A), a 0.5 A fuse for arrays from two- to five-strings (I_{GFPD}=0.566 to 1.05 A), and a 1 A fuse for larger arrays.

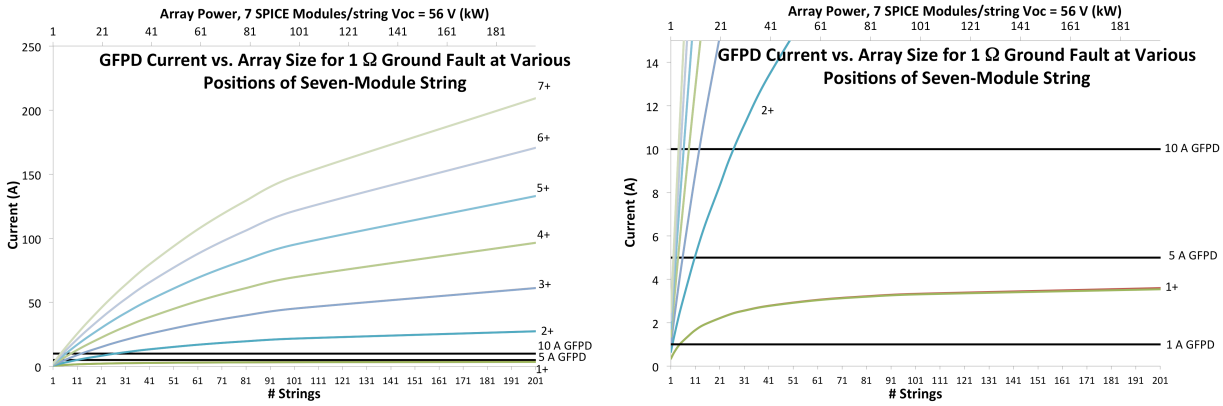

Figure 24: (left) GFPD current vs. array size for 1 Ω fault at various positions. The GFPD current is clearly sub-linear with respect to array size. For large array sizes, the load resistance is small enough compared to the fault resistance to divert a significant amount of current from the GFPD through the load. (right) Close-up view of the 2+ and 1+ fault positions. The 1+ fault position has a sub-linear dependence on array size as seen for the 0.01 Ω fault with a smaller slope at large array sizes. For larger array sizes, a 5 A fuse would be insufficient to catch such a fault, so a smaller fuse size must be used.

A final set of simulations was carried out for a 25 Ω fault at positions 1+ through 7+ with module leakages of 100 μA/module (Figure 25, top). The GFPD current is sub-linear for all faults at this resistance. This is due to the increased fault resistance. The fault resistance is now smaller than the load resistance for large array sizes so, as the number of strings increases, the current through the GFPD stays nearly constant while current through the load increases.

Figure 25 (bottom) shows a blown-up view of the 2+ and 1+ faults. The 1+ fault line shows a clear difference between the no leakage (green trace) vs. "nominal" 100 μA/module leakage (red trace). The offset for the "nominal" leakage case is due to the leakage current (blue trace). Due to the increased fault resistance, the GFPD current is lower than either the 0.01 Ω or 1 Ω case. In order to fully protect a PV system from a 25 Ω fault, it would be required to have a 0.25 A fuse for 1- and 2-string arrays (I_{GFPD}=0.30 and 0.45 A). If there were extremely high module leakage currents, e.g., 1 mA (~53.3 times larger than the IEC 61215 requirement for c-Si modules), a 0.5 A fuse would be needed for larger arrays, but almost certainly a 0.25 A fuse would not experience nuisance tripping from leakage current alone, shown by the 100 μA blue trace in Figure 25 (right). A 1 A fuse is too large for this 25 Ω fault resistance and would not be sufficient protection to clear the 1+ fault.

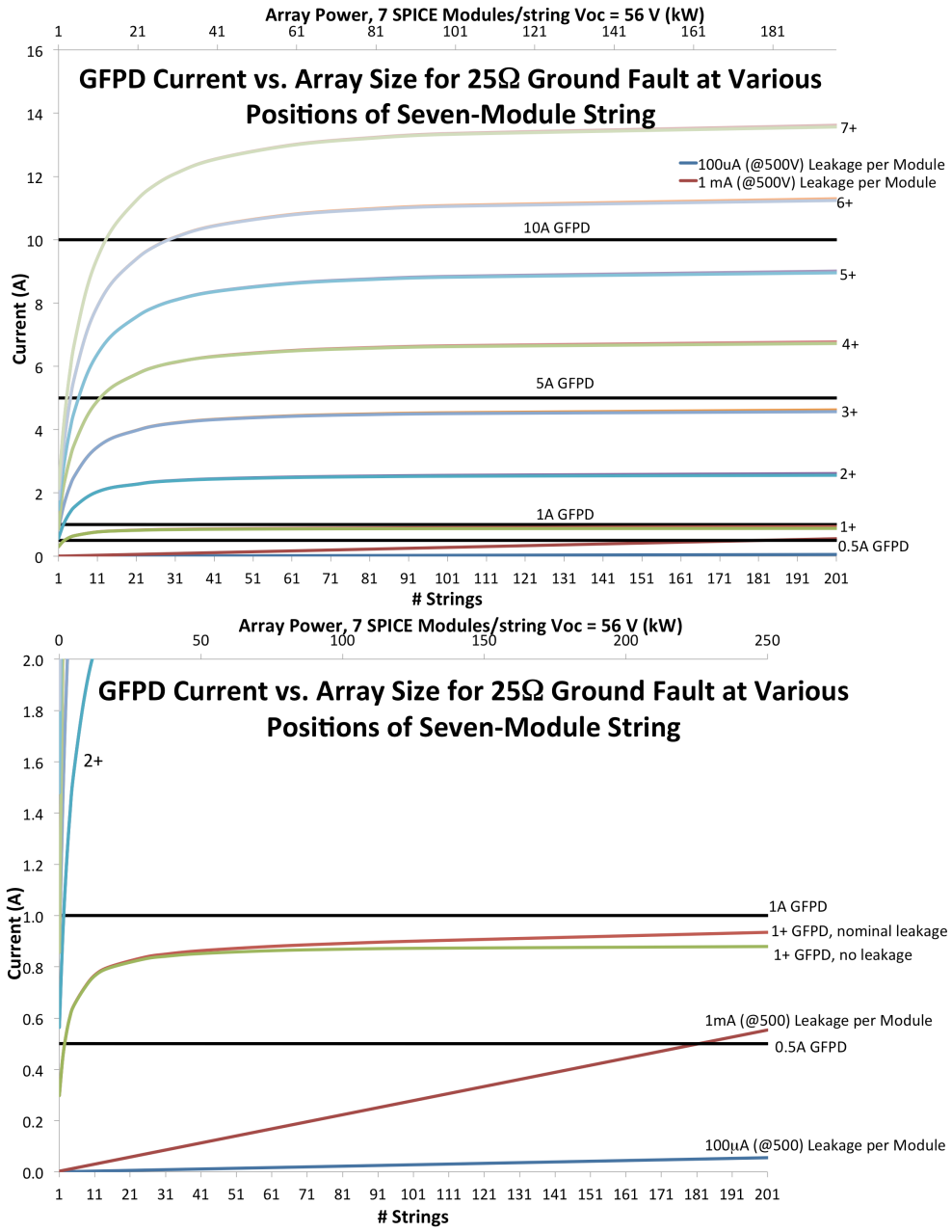

Figure 25: (top) GFPD current vs. array size for 25 Ω fault at various positions. The GFPD current is highly sub-linear with respect to array size. The load resistance is small compared to the fault resistance so, as more strings are added, current is diverted from the GFPD through the load. (bottom) Close-up view of the 2+ and 1+ fault positions. The 1+ fault position has a sub-linear dependence on array size as seen for the other fault cases with a smaller slope at large array sizes. For larger array sizes, a 1 A fuse would be insufficient to catch such a fault, so a smaller fuse size must be used.

It is apparent from the previous figures that GFPD current is highly dependent on fault resistance. To better understand this relationship, a series of simulations were carried out for arrays of different sizes with faults (R_{fault}=1 μΩ to 1000 Ω) at 1+. The results are shown in Figure 26. Figure 26 shows the GFPD current vs. array size for a 1+ fault of various fault

resistances for one through 201-strings (left) and one through 21-strings (right). All of the traces are sub-linear, however, the degree of GFPD current varies widely. For fault resistances close to a short circuit ($R_{fault}=1{\cdot}10^{-6}$ Ω), the GFPD current can be almost 4.5 A. However, for fault resistances as low as 1 Ω, the GFPD current drops to 3.5 A. Ideally, the GFPD rating would be above the leakage current but below all the potential fault currents. However from a practical standpoint, making the fuse rating sensitive enough to detect 1 kΩ faults (a 0.05 A fuse) introduces the system to nuisance tripping from transient noise in the system due to inverter transistor switching, MPPT, anti-islanding pulses, RF and antenna effects, and conducted noise from the AC side of the inverter. These have been measured in real systems at multiple times the steady-state leakage current [13]. While the slow-blow GFPD has some immunity to these transients, GFPDs must be selected to provide robustness to multiple sources of nuisance trips. Therefore, not all the high-impedance faults will be detectable, but a balance must be struck between minimizing nuisance trip issues and detecting the largest number of ground faults.

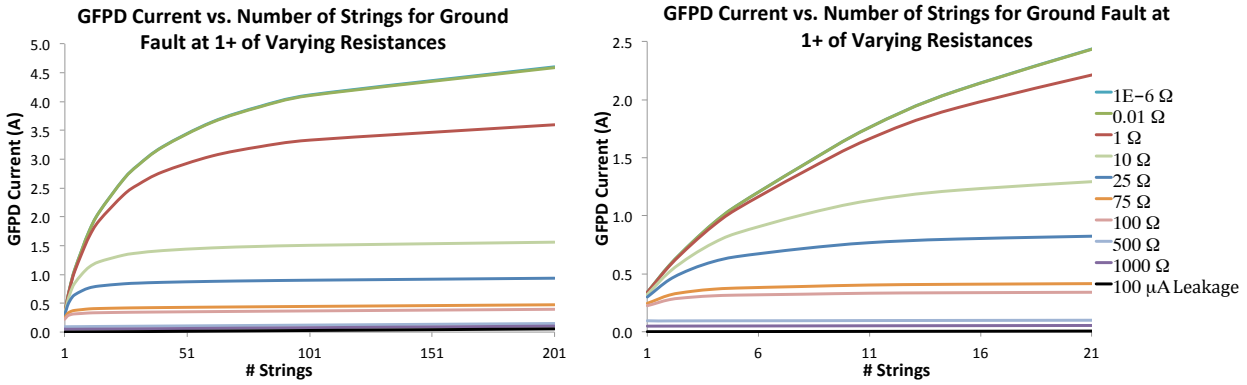

Figure 26: (left) GFPD current vs. array size for 1+ fault with various resistances. The GFPD current can vary widely, from 4.5 A for a short circuit to less than 0.5 A for a 75 Ω fault. The GFPD current drops rapidly as fault resistances increases. (right) Close-up of GFPD current vs. array size for 1+ fault for a single string array through a 21-string array.

Figure 27 shows the GFPD current vs. fault resistance for a single-string (left) and 101-string array (right) with a 1+ ground fault. GFPD current shows a $1/R_{fault}$ dependence for both cases. A 0.25 A fuse would be sufficient to detect faults below 75 Ω, but lower fuse ratings would be needed to protect against faults with a larger resistance. For the 101-string case, there is a steep drop in GFPD current for even slight increases in fault resistance above short circuit (0 Ω fault). Lower fuse ratings are needed to protect against these fault resistances. For any faults with resistances on the order of 10 Ω or above, a 1 A fuse may not be small enough to detect a 1+ fault on the 101-string array.

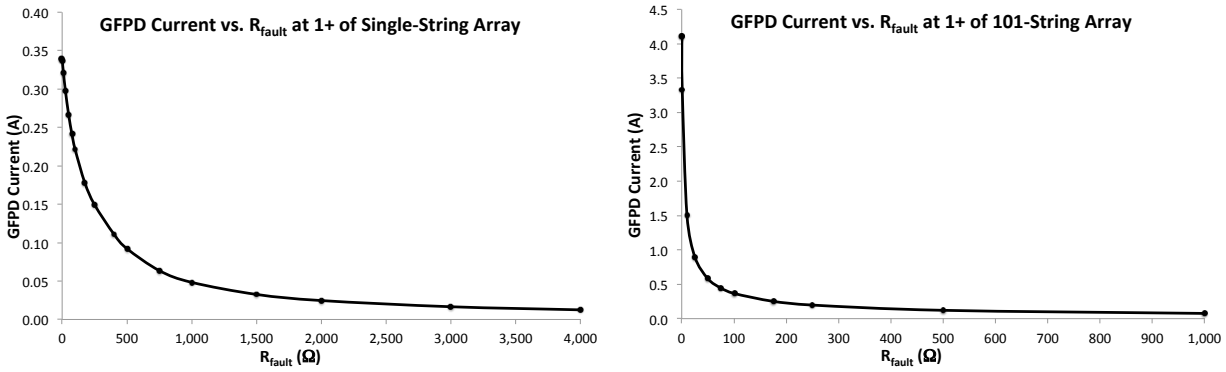

Figure 27: GFPD current vs. fault resistance for a 1+ fault of a single string (left) and 101-string (right) array. The GFPD current has a $1/R_{fault}$ dependence. For the single-string case, the GFPD current decreases for small increases in R_{fault} above short circuit. In the 101-string case, the GFPD current decreases precipitously for even small increases of R_{fault} above a short circuit.

5.6. Real-life ground fault resistances

Unfortunately, there is little known about the probability or progression of different fault impedances. With better understanding of the distribution of ground faults resistances, the fuse ratings could be selected for specific percentiles of protection. Without this knowledge, PV system designers are left to try to protect for as many fault cases as possible. This said, it stands to reason that undetectable, high-impedance faults will degrade over time, reducing their impedance to the point of detection. For this reason, it may not be critical to detect the high-impedance faults, as the currents produced by the fault in the EGC (equipment grounding conductors, i.e., racking, ground conductors, etc.) are not sufficient to cause injury and may eventually become detectable.

Without more experimental information, it is not possible to know what resistances would normally be seen in a ground fault. Faults could easily range from sub-1 Ω resistances (such as when conduit fittings cut through the cable insulation) to relatively large resistances (such as in corrosion bridging or insulation damage). However, to ensure faults, especially those occurring at 1+, are diagnosed immediately, the fuse size of GFPD should be kept low. While this increases the fault detection window, it makes the array more susceptible to nuisance tripping. Therefore, to fully protect PV arrays during humid and wet conditions while reducing nuisance tripping, a carefully selected fuse above the wet leakage current of the array must be employed. Reducing the fuse ratings would improve protection against the wide variety of possible ground faults.

5.7. Reducing GFPD fuse ratings reduces fault protection sensitivity

In the ideal case, fuse ratings could be decreased freely without affecting the GFPD current. However, in reality, fuse impedance is correlated to fuse rating. Figure 28 shows a graph of fuse resistance vs. fuse rating for a number of 10x38mm style fuses from a variety of manufacturers.

The resistance of the fuse is inversely proportional to the fuse rating so fuses with low ratings can have significant resistances. For example, the Littelfuse KLKD fuse has a resistance of 85.5 Ω for a 0.1 A fuse. Such large resistances can have significant effects on the GFPD current and fuse resistance must be balanced with fuse trip point in order to maximize GFPD fault detection capabilities.

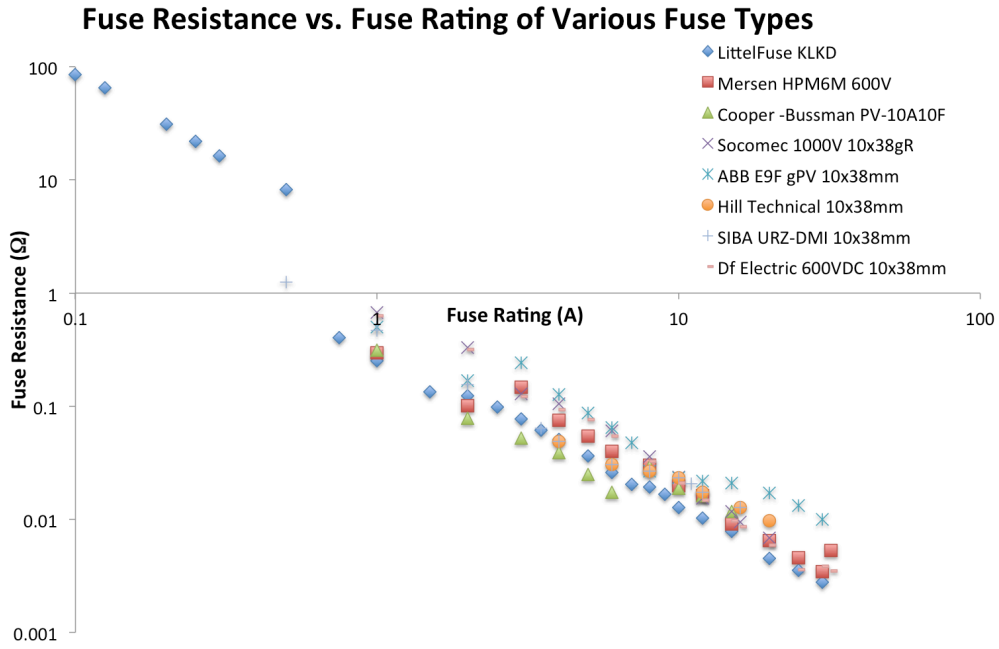

Figure 28: GFPD resistance vs. rating for a variety of 10x38 mm ("midget") fuses by various PV fuse manufacturers. In general, the more sensitive the fuse, the higher the intrinsic resistance [10, 19-25].

Table 2: KLKD fuse resistance and trip points used in SPICE simulations [10].

Fuse rating	Fuse Resistance (Ω)
5	0.0363
2	0.124
1	0.252
0.5	8.16
0.25	22.0
0.1	85.5

In order to investigate the effect of GFPD resistance on GFPD current, a 1+ ground fault was simulated with fault resistances of 0.1, 1, and 25 Ω on array sizes ranging from one to 301-strings. GFPD resistances and ratings were taken from the Littelfuse KLKD datasheet (Table 2). Figure 29 shows the results of these simulations. The left graph shows the data for fault resistances of 0.1 (dashed trace) and 1 Ω (dotted trace) with colors indicating fuse trip point. The solid traces indicate GFPD current at the fuse trip point.

As can be seen from Figure 29, when the fuse rating decreases (and GFPD resistance increases), the GFPD current decreases for a given value of R_{fault}. The GFPD current never increases above

5 A, so a 5 A fuse (orange) would not trip. All of the other fuse ratings (2 A, 1 A, 0.5 A, 0.25 A, and 0.1 A) would trip under these fault conditions. However, if the fault resistance is increased to 25 Ω (Figure 29, bottom), the GFPD current is less than 1 A for all fuse ratings. In this case, only the 0.5 A, 0.25 A, and 0.1 A fuses would trip. This indicates that, even taking into account fuse resistance; it is advantageous to move to sub-1 A GFPD ratings in order to detect higher impedance faults. The module leakage (black trace) is defined by a module leakage of 100 μA per module (5.3 times the maximum allowable IEC leakage for a 1.5 m^2 module).

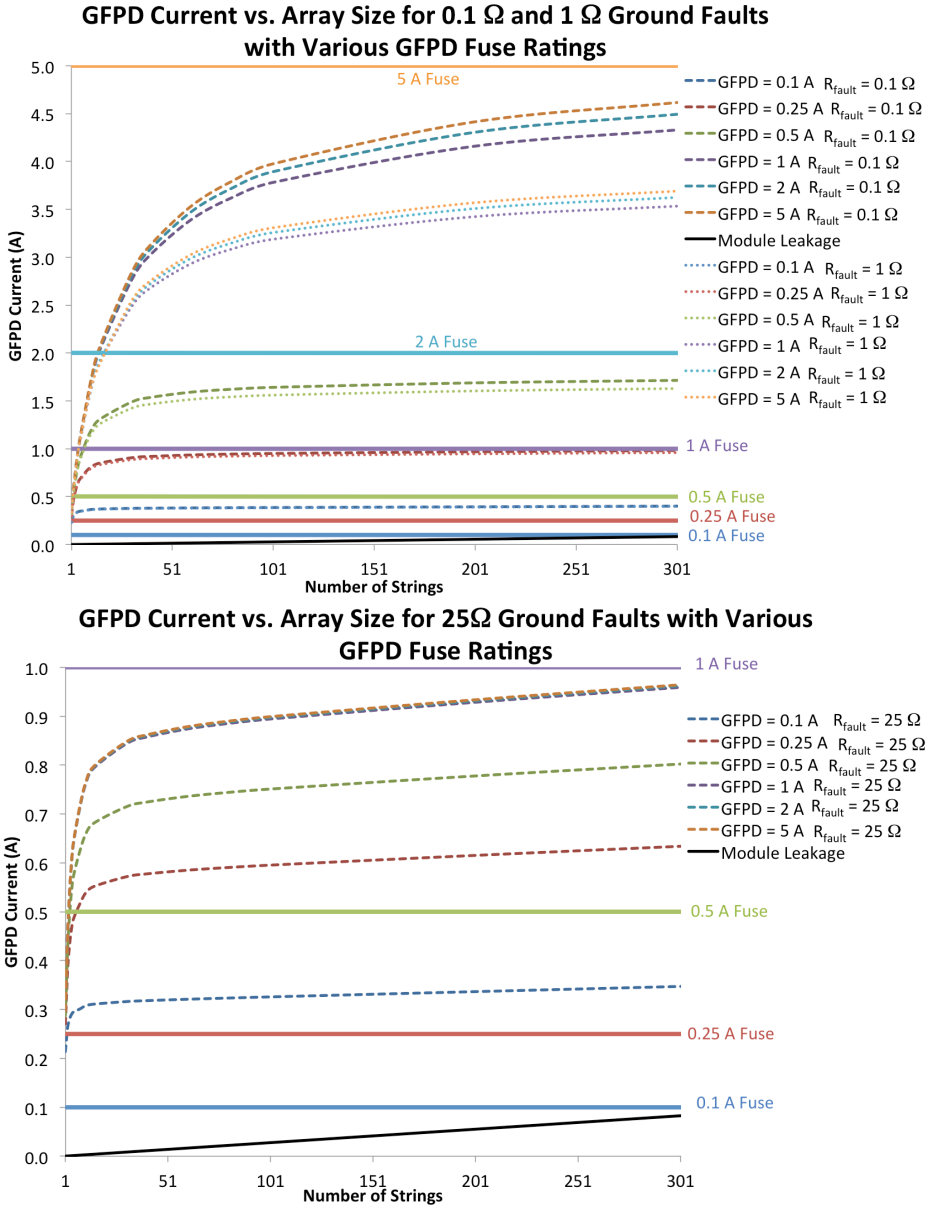

Figure 29: (top) GFPD current vs. array size for a 1+ ground fault with GFPDs of various resistances. As GFPD rating decreases (resistance increases) the GFPD current decreases. For 0.1 or 1 Ω faults, only the 5 A GFPD would not trip. (bottom) However, if the fault resistance is increased to 25 Ω, only the sub-1 A GFPDs would trip. This indicates that even though small fuse ratings have higher resistances, they still have greater detection capabilities for 1+ faults.

5.8. Influence of Overcurrent Protection on Large Systems

Another undetectable fault can exist in PV systems if the overcurrent protection device (OCPD) is less than the GFPD. In this case the OCPD clears before the GFPD has a chance to shut down the inverter and the fault is sustained indefinitely.

NEC 690.9 requires overcurrent protection for PV circuits in order to prevent conductors from exceeded their rated ampacity and starting fires. This could occur if the backfed current exceeds the current-carrying capacity of the conductors. In the case of systems with three or more strings, overcurrent fuses are required for each of the strings and typically selected to be the next highest fuse rating above $1.56 \cdot I_{sc}$ (125% of the string current, defined as 125% of the module short circuit current), or a 4 A OCPD fuse for the simulated strings in this document. Thus, for cases where the GFPD is rated for 5 A, it is possible the backfed current will clear the OCPD before the GFPD. At this point, the fault path is no longer being fed with the other strings, but there is still a fault path through the GFPD.

Figure 30 shows a 101-string array with a 0.1 Ω fault at 2+ of string 1. Prior to a protection device trip, 32.8 A flows through the GFPD and 30.3 A flows through the OCPD. The un-faulted modules (A) have been moved off MPP towards the short circuit condition. The modules above the fault in the faulted string (B) have been moved to voltages much higher than V_{oc} to accommodate the backfed current. Modules below the fault (C) are very near the short circuit condition.

If the OCPD possesses a smaller rating than the GFPD, it is possible for the OCPD to open before the GFPD, even though more current flows through the GFPD ($I_{GFPD}=I_{OCPD}+I_{sc}$). Which fuse will clear is dependent on the characteristic time-current curve of the device. If 4 and 5 A Littelfuse KLKD fuses are used in the OCPD and GFPD, respectively, 30.3 A through the OCPD will cause the smaller fuse to trip after 0.03 s, while the 32.8 A through the GFPD will not trip the fuse until 0.04 s. This time difference between fuse clearing events introduces the possibility of the OCPD fuse clearing before the GFPD fuse.

The case where the OCPD clears before the GFPD is shown in Figure 31 and could lead to a persistent, un-cleared fault condition. In this case, the OCPD trips due to the 30.3 A of current flow through the string, eliminating the backfed current through the faulted string. When the OCPD clears, the operation point of the un-faulted strings (A) moves towards MPP. The operation point is not quite at MPP because the inverter impedance is set to 101, not 100, strings in the simulation. The modules above the fault (B) are effectively at V_{oc} while the modules below the fault (C) are effectively short-circuited. These short-circuited modules continue to source current through the fault and the GFPD, though the magnitude of the current is equal to I_{sc}. Since this new fault current is much less than the GFPD trip point, the fault will persist.

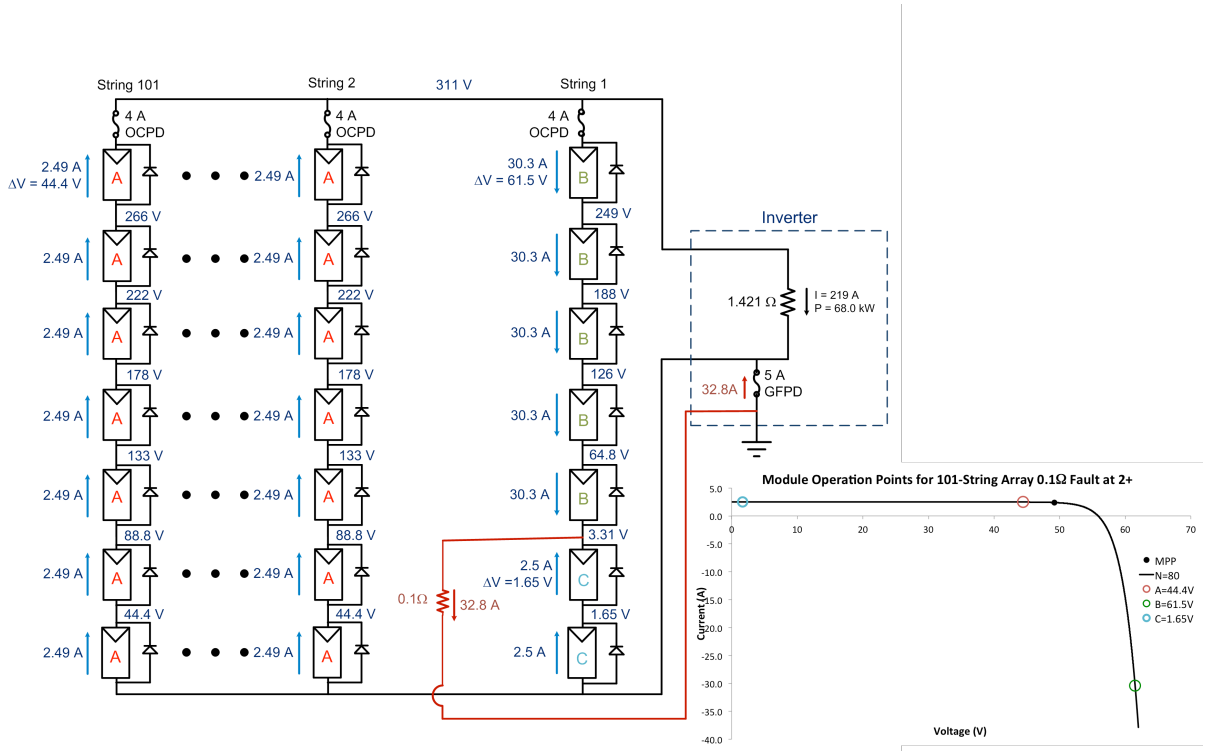

Figure 30: Example of a low resistance ground fault at 2+ in a 101-string array. The modules in the unfaulted strings (A) have moved off MPP towards short circuit. The unfauled strings backfeed current through the modules above the fault (B). This causes those modules to have an applied voltage larger than V_{oc}. The modules below the fault (C) move close to short circuit conditions.

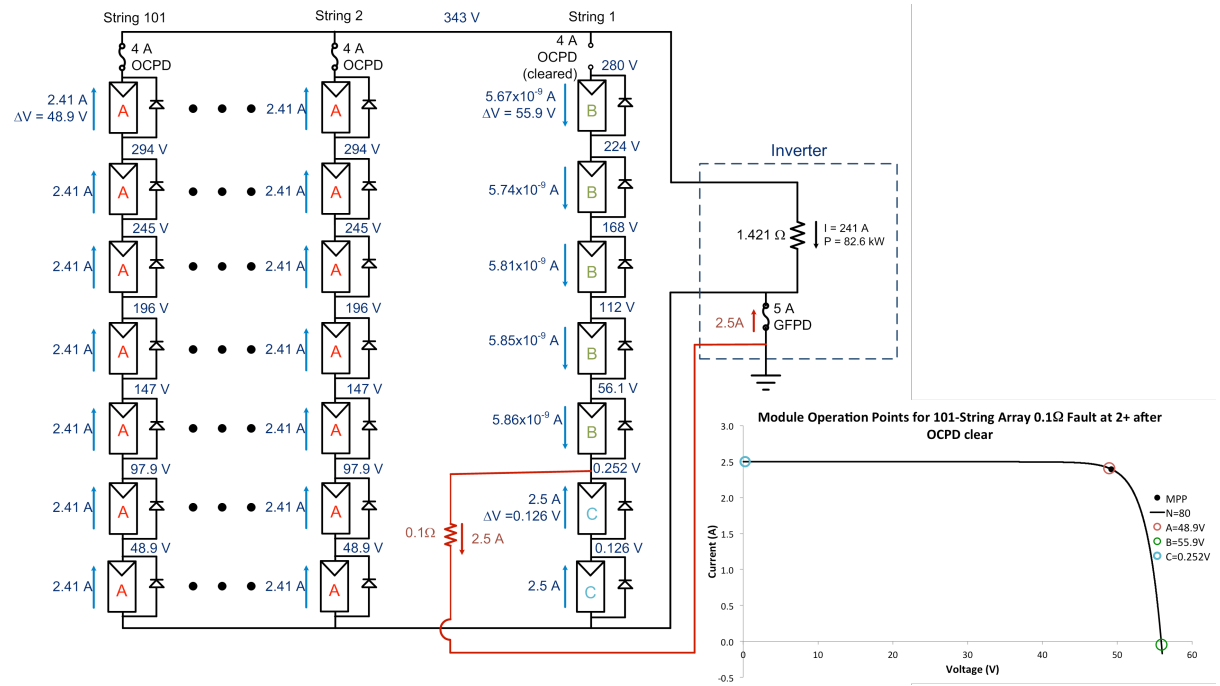

Figure 31: Example of a ground fault that clears the OCPD but not the GFPD because the ground fault fuse has a higher rating than the overcurrent fuse. After the OCPD clears the fault remains energized and undetected.

This case illustrates the care that must be taken when designing the GFPD. In section 5, it was demonstrated that IEC-compliant module leakage would not cause nuisance tripping, even for GFPD ratings as low as 1 A in 100 kW systems. The case where the OCPD clears before the GFPD indicates that:

- a small (less than string I_{sc}) GFPD rating should be used, and
- the characteristic clear time of the GFPD should be less than the OCPD.

This page is intentionally left blank.

6. DETECTION OF "BLIND SPOT GROUND" FAULTS WITH GFPDS

Recently, a detection limit, or "blind spot," in traditional ground fault protection systems has been identified for the DC-grounded, AC-isolated PV systems, most common in the United States [17]. This blind spot occurs when the grounded current-carrying conductor (CCC) is faulted to the equipment grounding conductor (EGC) as shown in Figure 32.

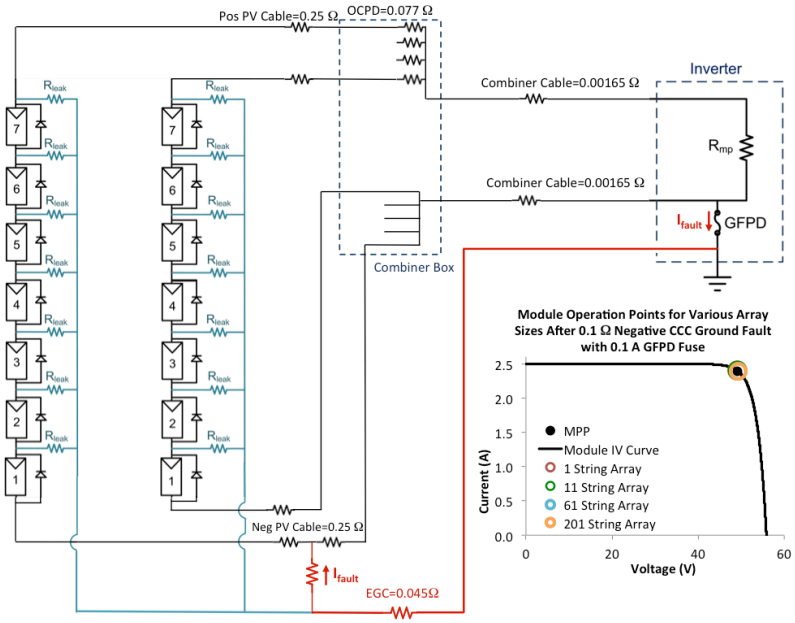

Figure 32: Schematic for an array with parasitic impedances measured from a fielded system and non-zero GFPD impedance. The teal line denotes the leakage current path. The path of the ground fault on the negative CCC is denoted in red.

These faults may produce small fault currents that can go undetected by GFPDs. The danger of undetected ground faults in the EGC is twofold:

1. an energized EGC can be a shock hazard, resulting in severe injury; and

2. if there is a second ground fault, the array can be shorted though the EGC, bypassing the GFPD and allowing fault current to flow undetected through the system with no means of interruption.

The fires presented in [1, 26] have highlighted the incomplete protection provided by ground fault fuses in grounded arrays in the United States. Field experiments have confirmed the existence of the ground fault blind spot in grounded systems [13]. However in ungrounded, non-isolated, and hybrid systems the ground fault blind spot does not exist.

In this study, we develop an analytical and numerical SPICE model for PV systems that have a ground fault between the grounded CCC to the EGC. These models are used to perform electrical

simulations of faults occurring on arrays of various sizes (representing residential, commercial, and utility scale systems) with different fault, cabling, and GFPD impedances.

6.1. Conductor resistances in PV arrays

To model current flow during a ground fault, the internal resistances of the conductors and the GFPD must be included because the current division between the fault path and the intended conduction path is heavily dependent on small internal resistances. In the ideal case, fuse ratings could be decreased freely without affecting the GFPD current. However, in reality, fuse impedance changes with fuse ampere rating (Figure 28). UL 1741 [18] mandates the maximum sizing of these protection devices based on the array size, as shown in Figure 20. The resistance of the fuse is inversely related to the fuse rating. Fuses with low trip ratings can have significant resistances. For example, the 0.1 ampere (A) Littelfuse KLKD fuse has a resistance of 85.5 Ω. Such large resistances have significant effects on the GFPD current during a fault and fuse resistance must be balanced with fuse trip point in order to maximize GFPD fault detection capabilities. As will be seen below, this effect is much more severe in blind spot faults than to ground faults to 1+ through 7+, shown in Section 5.7.

GFPD impedance means that the grounded CCC (typically the negative conductor) is no longer at ground potential, but instead *functionally* grounded by the fuse. When a fuse with internal resistance is included in the model of a PV system, the conductor is at a voltage above ground potential, which introduces the possibility of ground faults from the grounded CCC through the EGC.

6.2. SPICE simulations with parasitic cable/fuse impedances

A new SPICE model was created with the internal resistance of the conductors and GFPD fusing, as shown in Figure 32, in order to investigate ground faults involving the grounded CCC. As in previous simulations, each string was composed of seven modules having a leakage current to ground determined by R_{leak} ("nominal" leakage chosen to be 100 μA/module at 500 V bias). Array sizes of one to 201 strings were simulated with each DC home run cable from the PV to the combiner box totaling 0.25 Ω (~80 ft of coated copper 12 AWG cabling). Prior to each string being combined, the positive DC cable was connected to an OCPD with 0.077 Ω resistance (4 A fuse rated for $1.56 \cdot I_{sc}$). The combiner box was connected to the inverter through cabling with an impedance of 0.00165 Ω (~50 ft of coated copper 400 kcmil cabling). The ground fault was modeled by a resistor connected from the negative CCC to ground through the 0.045 Ω EGC (determined from field measurements [13]). On the faulted string in Figure 32, the PV cabling resistance was split by the fault. This was done so that, by altering the resistance before and after the fault, the position of the fault in the PV cabling could be varied. The value of the inverter resistor was set to the max power point of the unfaulted array. The negative inverter connection was connected to ground through the GFPD.

In the fault condition shown in Figure 32, the operating points of the modules do not move from MPP due to the blind spot fault. It should be noted that the fault current is in the opposite direction of the leakage current, shown in Figure 33. This indicates that in arrays with large leakage currents, it is more difficult for the GFPD to detect a blind spot ground fault because the fault current must first reverse the leakage current. Note that for these simulations—as before—the current sign convention is such that current through the GFPD from EGC to grounded CCC is taken to be positive.

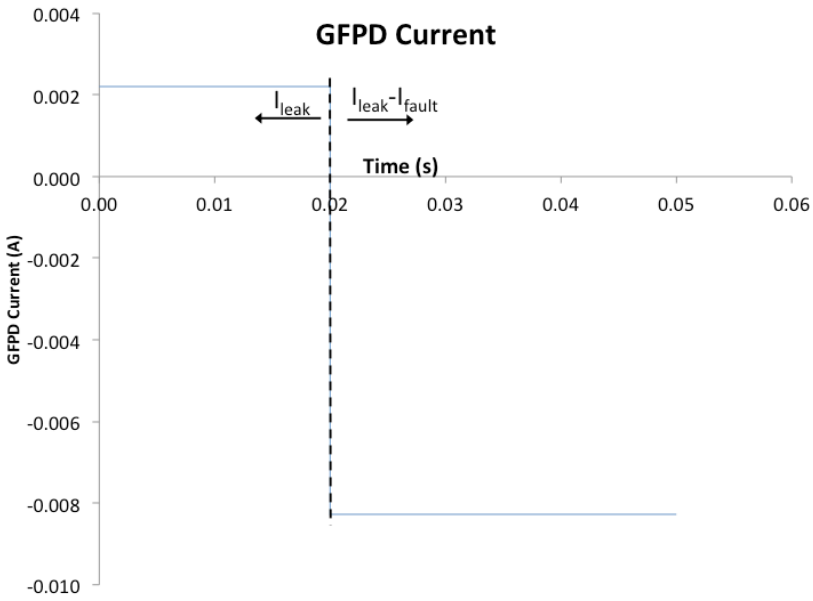

Figure 33: Graph of GFPD current vs. time for a SPICE simulation of a fault from the negative CCC to ground. The array is faulted at 0.02 seconds. Before the fault, leakage current flows from ground to the negative CCC through the GFPD. After the fault, current flows through the GFPD in the opposite direction.

6.3. Analytical solution to "blind spot" ground fault currents

Through circuit analysis, the GFPD current can be shown to be a function of the module maximum power current (I_{mp}), number of strings (C), wiring resistance (R_{comb}, R_{EGC}, etc), resistance of the faulted portion of the PV cabling (R_x), fault resistance (R_{fault}), GFPD resistance (R_{GFPD}), and the array leakage current (I_{leak}).

The circuit diagram in Figure 34 shows the current paths for a single string that has a fault in the grounded negative CCC at some point in the PV cabling. The fault bisects the PV cable at some arbitrary point and acts as voltage divider. R_x denotes the resistance of the PV cabling included in the fault loop, while R_y denotes the portion of PV cabling resistance that is not included in the fault loop. The sum of R_x and R_y is equal to R_{PV} and the ratio of the two resistances is equal to the percentage of PV cabling that is faulted.

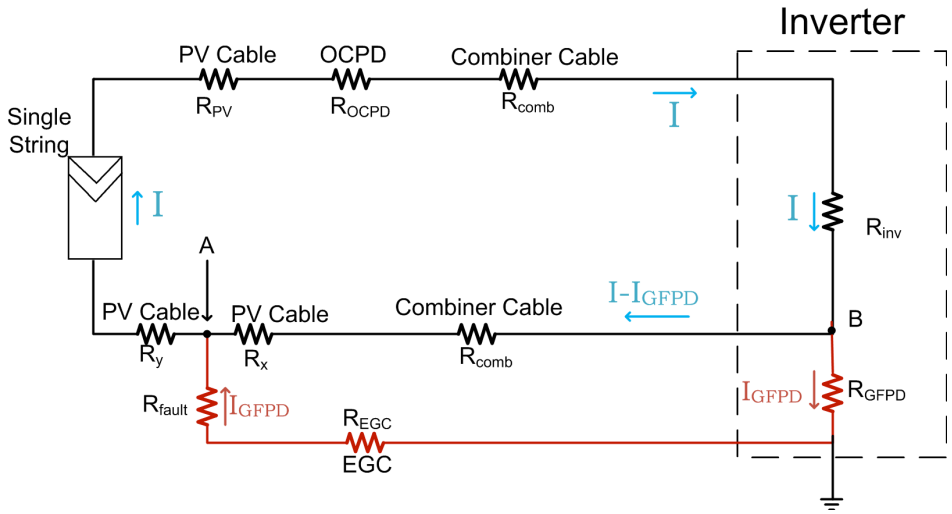

Figure 34: Circuit diagram of negative CCC fault with a single string at an arbitrary point in the negative PV cabling. The ratio of R_x and R_y indicates the percentage of PV cabling faulted. Resistances and currents used in Kirchoff's Voltage Law equations are shown.

The inset graph in Figure 32 shows the module operating point for various array sizes after the fault. The location of the PV modules on their IV curve is nearly unchanged due to the blind spot fault, so the string current is treated as constant in the following analytical analysis. By Kirchoff's Current Law (KCL), current is conserved at circuit junctions. Also, by Kirchoff's Voltage Law (KVL), the sum of voltages in a closed loop is always equal to zero:

$$\sum_{k=1}^{n} V_k = 0 \tag{6}$$

This implies that the voltage drop between points A and B is equivalent regardless of the current path. By Ohm's Law, the voltage drop between A and B can be written as:

$$\Delta V_{A,B} = I_{GFPD} \cdot \left(R_{GFPD} + R_{EGC} + R_{fault}\right) = \left(I - I_{GFPD}\right) \cdot \left(R_{comb} + R_x\right) \tag{7}$$

By distributing and refactoring in terms of I and I_{GFPD} and solving for I_{GFPD}, Equation (7) can be written as:

$$I_{GFPD} = \frac{I \cdot \left(R_{comb} + R_x\right)}{\left(R_{GFPD} + R_{EGC} + R_{fault} + R_{comb} + R_x\right)} \tag{8}$$

As shown in the simulations previously, the operating point of the modules on the IV curve are nearly unaltered during a negative CCC ground fault. Therefore:

$$I = I_{mp} \tag{9}$$

and,

$$I_{GFPD} = \frac{I_{mp} \cdot \left(R_{comb} + R_x\right)}{\left(R_{GFPD} + R_{EGC} + R_{fault} + R_{comb} + R_x\right)} \tag{10}$$

Next, consider the case of a negative CCC fault with multiple strings. Figure 35 shows a circuit schematic for an array composed of multiple strings with a negative CCC fault at a single string. The module symbol on the left indicates a single string while the module symbol on the right is a stand-in for (C-1) parallel strings. This is a slightly more complicated problem because this fault diverts current away from the negative CCC path (I_1) through the unfaulted strings (I_2).

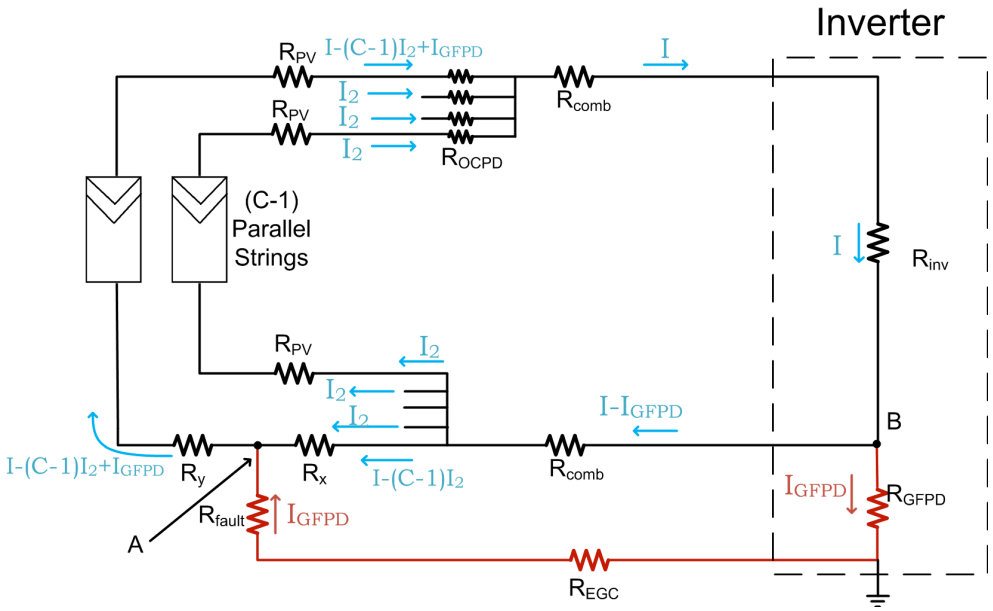

Figure 35: Circuit diagram of negative CCC fault of an array with a number (C) of parallel strings and a fault at some arbitrary point in the negative PV cabling. The ratio of R_x and R_y indicates the percentage of PV cabling faulted. Resistances and currents used in KVL equations are shown.

The results of KVL circuit analysis on this circuit are similar to Equation (8) and the GFPD current can be described by:

$$\left(I - I_{GFPD}\right) \cdot R_{comb} + I_1 \cdot R_x = I_{GFPD} \cdot \left(R_{GFPD} + R_{EGC} + R_{fault}\right) \tag{11}$$

As in the previous derivations, it is fortuitous that the module operating points do not change due to the negative CCC fault. Because of this, the current through the strings is the same before and after the fault and I, I_1, and I_2 can be described by:

$$I = C \cdot I_{mp} \tag{12}$$

$$I_1 + I_{GFPD} = I_{mp} \tag{13}$$

This allows Equation (11) to be rewritten as:

$$\left(C \cdot I_{mp} - I_{GFPD}\right) \cdot R_{comb} + \left(I_{mp} - I_{GFPD}\right) \cdot R_x = I_{GFPD} \cdot \left(R_{GFPD} + R_{EGC} + R_{fault}\right) \tag{14}$$

Finally, by regrouping terms and solving for I_{GFPD}, Equation (14) can be reduced to:

$$I_{GFPD} = \frac{I_{mp} \cdot \left(C \cdot R_{comb} + R_x\right)}{\left(R_{GFPD} + R_{EGC} + R_{fault} + R_{comb} + R_x\right)} \tag{15}$$

The circuit schematic depicted in Figure 35 is the type of circuit used in the simulations. However, it is usually only representative for ≤50 string arrays because larger arrays often contain recombiners, shown in Figure 36. Groups of strings are wired together into a combiner box and then recombined before being connected to the inverter.

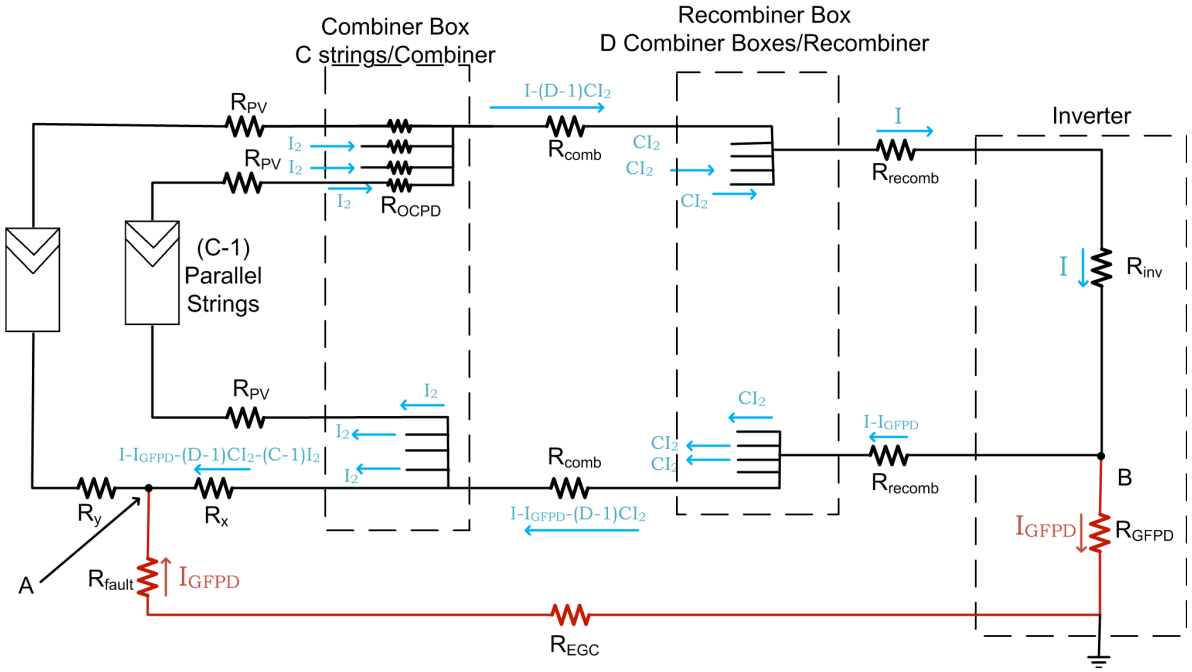

Figure 36: Circuit diagram of negative CCC fault of an array with a number (C) of multiple parallel strings, which are wired into a combiner box. D combiner boxes outputs are then wired into a recombiner box. A fault occurs at some arbitrary point in the negative PV cabling of a string. The ratio of R_x and R_y indicates the percentage of PV cabling faulted. Resistances and currents used in KVL equations are shown.

In this case, the KVL can be described by:

$$\begin{aligned} &I_{GFPD} \cdot R_{GFPD} + I_{GFPD} \cdot R_{EGC} + I_{GFPD} \cdot R_{fault} = \\ &\left(I - I_{GFPD}\right) \cdot R_{recomb} + \left[I - I_{GFPD} - \left(D-1\right) \cdot C \cdot I_2\right] \cdot R_{comb} + \left[I - I_{GFPD} - \left(D-1\right) \cdot C \cdot I_2\right] \cdot R_x \end{aligned} \tag{16}$$

This equation can be simplified because the strings remain at their maximum power by:

$$I = D \cdot C \cdot I_{mp} \tag{17}$$
$$I_2 = I_{mp}$$

So that Equation (16) can be simplified to:

$$I_{GFPD}\left(R_{GFPD} + R_{EGC} + R_{fault}\right) = \left(D \cdot C \cdot I_{mp} - I_{GFPD}\right) \cdot R_{recomb} + \left[C \cdot I_{mp} - I_{GFPD}\right] \cdot R_{comb} + \left(I_{mp} - I_{GFPD}\right) \cdot R_x \tag{18}$$

Finally, the GFPD current can be found by simplifying and grouping to be:

$$I_{GFPD} = \frac{I_{mp}\left[D \cdot C \cdot R_{recomb} + C \cdot R_{comb} + R_x\right]}{R_{GFPD} + R_{EGC} + R_{fault} + R_{recomb} + R_x} \tag{19}$$

A simple check shows that if the number of combiner boxes per recombiner box is chosen as one or the recombiner resistance is set to zero, Equation (19) reduces to Equation (15).

For the more complicated array shown in Figure 36, there are three possible positions for a fault. The equation for a fault at some point in the string conductor between the array and the combiner is shown in Equation (19). A fault at the combiner means that R_x becomes zero and R_{comb} is redefined as R_x and R_y to give a GFPD current of:

$$I_{GFPD} = \frac{I_{mp}\left(D \cdot C \cdot R_{recomb} + C \cdot R_x\right)}{R_{GFPD} + R_{EGC} + R_{fault} + R_{recomb} + R_x} \tag{20}$$

This equation is further simplified for the case of a fault at the recombiner cabling. In this case, R_x and R_{comb} are both zero in Equation (19) and R_{recomb} is redefined as R_x and R_y to give a GFPD current equivalent to:

$$I_{GFPD} = \frac{D \cdot C \cdot I_{mp} \cdot R_x}{R_{GFPD} + R_{EGC} + R_{fault} + R_x} \tag{21}$$

The previous circuit analyses have all been carried out for perfect arrays. However, PV arrays have leakage currents. In the case of ground faults at the negative CCC, the leakage current flows in the opposition direction of the fault current (see, for example, Figure 37).

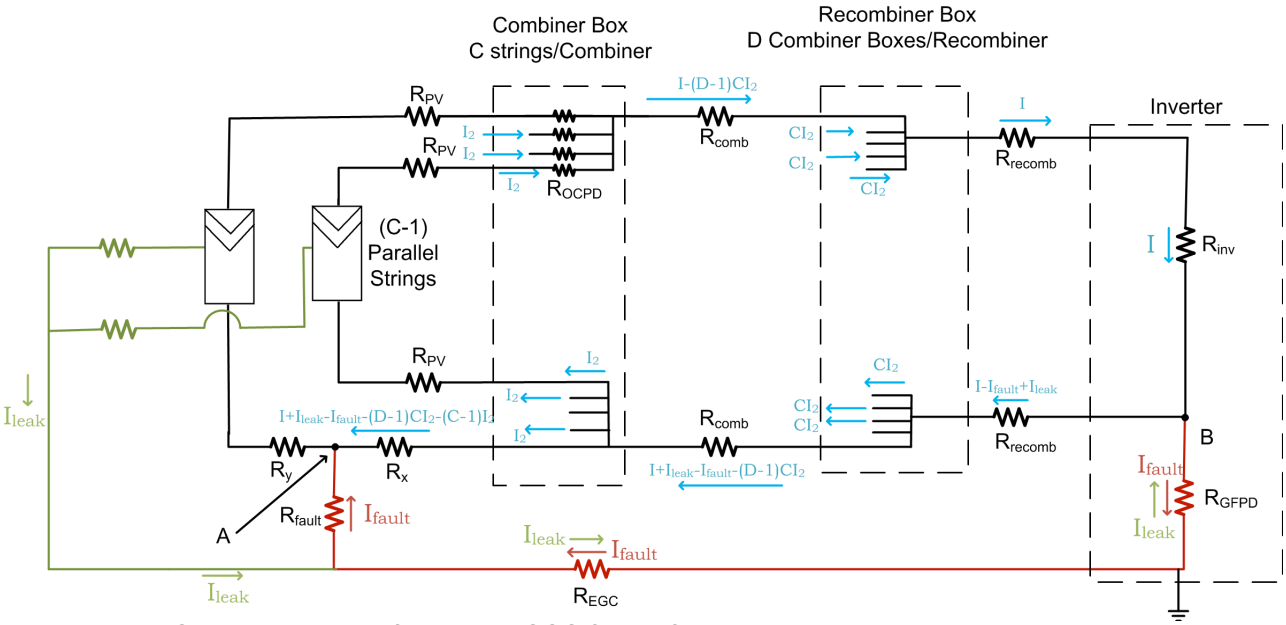

Figure 37: Circuit diagram of negative CCC fault of an array with leakage current. Resistances and currents used in KVL equations are shown.

The KVL analysis of the circuit between points A and B can be described by:

$$\begin{aligned}&\left(I+I_{leak}-I_{fault}\right)\cdot R_{recomb}+\left(I+I_{leak}-I_{fault}-\left(D-1\right)CI_2\right)\cdot R_{comb}+\left(I+I_{leak}-I_{fault}-(D-1)\cdot C\cdot I_2-(C-1)\cdot I_2\right)\cdot R_x\\&=\left(I_{fault}-I_{leak}\right)\cdot R_{GFPD}+\left(I_{fault}-I_{leak}\right)\cdot R_{EGC}+I_{fault}\cdot R_{fault}\end{aligned}\tag{22}$$

Again, the modules are at maximum power so they can be described by:

$$\begin{aligned}I&=D\cdot C\cdot I_{mp}\\I_2&=I_{mp}\end{aligned}\tag{23}$$

So Equation (23) can be inserted into Equation (22):

$$\begin{aligned}&\left(D\cdot C\cdot I_{mp}+I_{leak}-I_{fault}\right)\cdot R_{recomb}+\left(D\cdot C\cdot I_{mp}+I_{leak}-I_{fault}-D\cdot C\cdot I_{mp}+C\cdot I_{mp}\right)\cdot R_{comb}+\left(I_{mp}-I_{fault}+I_{leak}\right)\cdot R_x\\&=I_{fault}\cdot\left(R_{GFPD}+R_{EGC}+R_{fault}\right)-I_{leak}\cdot\left(R_{GFPD}+R_{EGC}\right)\end{aligned}\tag{24}$$

And solving for I_{fault}:

$$I_{fault}=\frac{I_{mp}\cdot\left(D\cdot C\cdot R_{recomb}+C\cdot R_{comb}+R_x\right)+I_{leak}\cdot\left(R_{recomb}+R_{comb}+R_x+R_{GFPD}+R_{EGC}\right)}{\left(R_{GFPD}+R_{EGC}+R_{fault}+R_{recomb}+R_{comb}+R_x\right)}\tag{25}$$

The GFPD current is the difference in the fault and leakage currents (and, by convention in these simulations, I_{fault} is taken to be negative), so I_{fault} can be transformed into I_{GFPD} by:

$$I_{GFPD} = I_{leak} - I_{fault} \tag{26}$$

Finally, Equation (25) can be solved in terms of I_{GFPD} by substituting Equation (26) into Equation (25):

$$I_{fault} = I_{leak} - \frac{I_{mp} \cdot \left(D \cdot C \cdot R_{recomb} + C \cdot R_{comb} + R_x\right) + I_{leak} \cdot \left(R_{recomb} + R_{comb} + R_x + R_{GFPD} + R_{EGC}\right)}{\left(R_{GFPD} + R_{EGC} + R_{fault} + R_{recomb} + R_{comb} + R_x\right)} \tag{27}$$

In the simulations, the recombiner topology is not used (D=1, R_{recomb}=0 Ω), so the equation for I_{GFPD} shown as Equation (27) becomes:

$$I_{GFPD} = I_{leak} - \frac{I_{mp} \cdot \left(C \cdot R_{comb} + R_x\right) + I_{leak} \cdot \left(R_{comb} + R_x + R_{GFPD} + R_{EGC}\right)}{\left(R_{GFPD} + R_{EGC} + R_{fault} + R_{comb} + R_x\right)} \tag{28}$$

6.4. Simulation results

For the purposes of this work, the one-diode model is constructed to approximate a nearly perfect photovoltaic module. The current source is set to supply 2.5 A at short circuit, the diode has an ideality factor of N=80, the shunt resistance is set $1 \cdot 10^{20}$ Ω and the series resistance is set to 10 mΩ. This module gives an IV curve with I_{sc} of 2.5 A, V_{oc} of 56 V, and P_{mp} of 118 W. The MPP has a current of I_{mp}=2.4 A and a voltage of V_{mp}=49.2 V. These values were chosen to approximate the operation of modules in a 600 V array at Sandia's Distributed Energy Testing Laboratory on a summer day.

The model of a PV array is composed of a number of strings in parallel (as many as 201). Each string is composed of seven modules in series. Each module is connected to a bypass diode ($I_{sat}=4.7 \cdot 10^{-12}$ A, N=1). The array is wired to a resistor, as a basic approximation of the real input impedance of an inverter. The resistance connected to the array in all the simulations is set at the resistance required to generate maximum PV power, R_{mp}, of the unfaulted array.

The SPICE model was created with the internal resistance of the conductors and GFPD fusing, as shown in Figure 32 in order to investigate ground faults involving the negative CCC. Arrays were simulated with each DC home run cable from the PV to the combiner box totaling 0.25 Ω (~80 feet of coated copper 12 American wire gauge (AWG) cabling at 3.125 mΩ/ft). Prior to each string being combined, the positive DC cable is connected to an overcurrent protection device with 0.077 Ω resistance (4 A KLKD Littelfuse [10] rated for $1.56 \cdot I_{sc}$). The combiner box is connected to the inverter through cabling with an impedance of 0.00165 Ω (~50 feet of coated copper 400 circular mil (kcmil) cabling at 0.033 mΩ/foot). The ground fault is modeled by a resistor connected from the negative CCC to ground through the 0.041 Ω EGC (determined from field measurements [13]). On the faulted string in Figure 32, the PV cabling resistance is split by the fault. This was done so that, by altering the resistance before and after the fault, the position of the fault in the PV cabling could be varied. The value of the inverter resistor is set to the MPP

of the unfaulted array. The negative inverter connection is connected to ground through the GFPD.

To investigate the effect of GFPD resistance on fault current, simulations were carried out for GFPD resistances of 85.5, 22, 8.16, 0.252, 0.124, and 0.0363 Ω (LittelFuse KLKD resistances for 0.1, 0.25, 0.5, 1, 2, and 5 A fuses [10], respectively) with fault resistances of 0.1, 1, and 25 Ω. Figure 38 shows the results of the simulations for 1, 2, and 5 A GFPD fuses and fault resistances of 0.1 and 1 Ω. Simulations with a 1 A (0.252 Ω), 2 A (0.125 Ω), and 5 A (0.0363 Ω) are shown as red, purple, and orange points, respectively. Triangles indicate a fault resistance of 0.1 Ω while circles represent a 1 Ω resistance. Solid lines at 1, 2, and 5 A denote the fuse ratings with color corresponding to the fuse trip point. The GFPD current calculated by Equation (28) is denoted by a dashed line for each set of fuse and fault resistances.

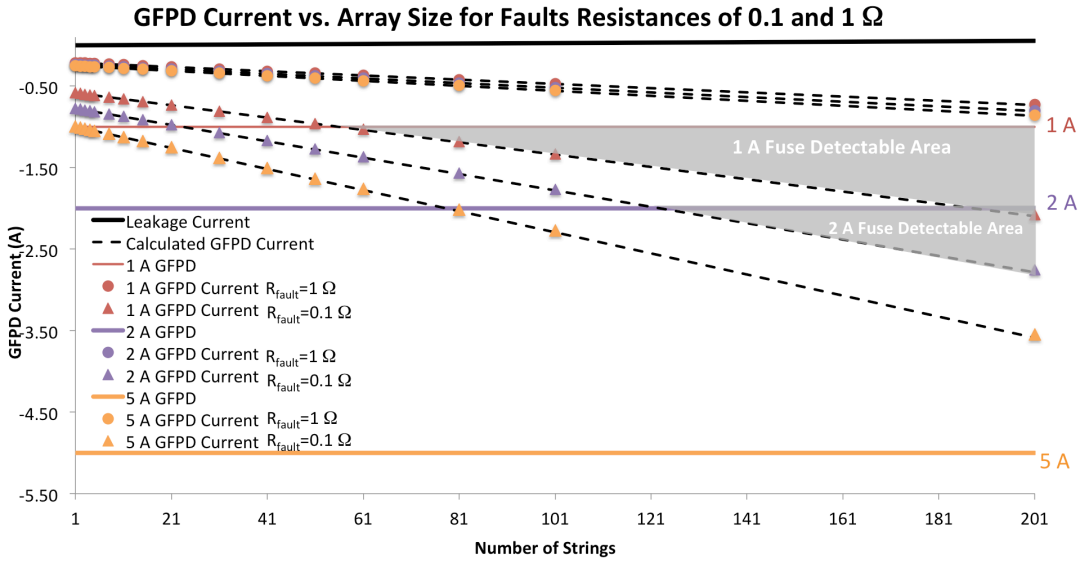

Figure 38: Graph of GFPD current vs. array size for various GFPD and fault resistances. The color of the line indicates GFPD resistance. Red traces denote 1 A (0.252 Ω), while purple and orange traces denote 2 A (0.124 Ω), and 5 A (0.0363 Ω), respectively. Only the 1 A and 2 A fuses are sensitive enough to trip due to the blind spot fault. The range in which I_{GFPD} is larger than the trip point is colored in gray.

The GFPD current is linear with the number of strings for all GFPD fuse ratings and fault resistances. Also, for all arrays up to 201 strings, only the 1 A and 2 A GFPDs (at fault resistance of 0.1 Ω) provide enough GFPD current to trip the fuse (colored regions denote where $I_{fault}>I_{GFPD}$). The 1 A GFPD only detects the ground fault in arrays larger than 56 strings while the 2 A GFPD detects faults in arrays larger than 124 strings. The orange traces do not reach 5 A even for 201 strings, so a 5 A GFPD would not trip for a blind spot ground fault of 0.1 or 1 Ω.

It is tempting to believe that decreasing the fuse rating will increase the number of detectable blind spot faults. However, the decrease in trip point is more than offset by the increased GFPD resistance, so fuses with low ratings will detect fewer blind spots. Figure 39 shows the simulation results for 0.1 (green), 0.25 (purple), and 0.5 A (blue) GFPD fuse ratings at R_{fault} of

0.1 and 1 Ω. In each case, due to the increase fuse resistance, the GFPD current is far too small to trip the fuses.

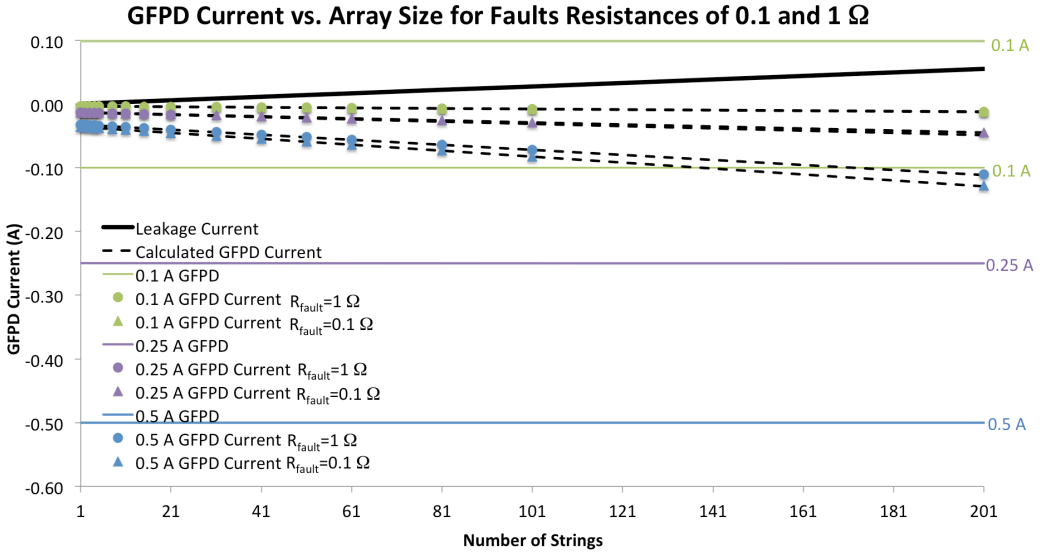

Figure 39: Graph of GFPD current vs. array size for various GFPD and fault resistances. The color of the line indicates GFPD resistance. Green traces denote 0.1 A (85.5 Ω), while purple and blue traces denote 0.25 A (22 Ω), and 0.5 A (8.16 Ω), respectively. Even though the fuses have low trip points, due to the increased fuse resistance, the GFPD current is below the fuse trip point and the blind spot window is increased.

Table 3 summarizes the simulation results for GFPD current at different fault resistance and fuse ratings. The color of the cell denotes whether it is possible to detect a blind spot fault. Only the 1 A and 2 A fuses at R_{fault}=0.1 Ω have the combination of low trip point and low fuse resistance needed to detect the blind spot fault for large array sizes (more than 56 and 124 strings, respectively). Thus, to limit the size of the blind spot, fuse rating and fuse resistance must both be considered and optimized.

Table 3: GFPD current for various fault resistances and fuse ratings. The color of the cell indicates if a blind spot fault is detectable. Only the 1 A and 2 A fuses (at R_{fault}=0.1 Ω) have both a low enough trip point and a low enough resistance to detect the blind spot fault for array sizes above 56 and 124 strings, respectively.

Fuse (A)	R_{fault} (Ω)	I_{GFPD} (A)	Min Number of Strings to Detect Fault (0.98 kW/string)
0.1	0.1	0.0126 A @ 201-string	>201
	1	0.019 A @ 201-string	>201
	25	0.00259 A @ 201-string	>201
0.25	0.1	0.0486 A @ 201-string	>201
	1	0.0446 A @ 201-string	>201
	25	00608 A @ 201-string	>201
0.5	0.1	0.0128 A @ 201-string	>201
	1	0.0111 A @ 201-string	>201
	25	0.00862 A @ 201-string	>201
1	0.1	1.00 A @ 56-string	56
	1	0.727 A @ 201-string	>201
	25	0.0113 A @ 201-string	>201
2	0.1	2.004 A @ 124-string	124
	1	0.801 A @ 201-string	>201
	25	0.0111 A @ 201-string	>201
5	0.1	3.56 A @ 201-string	>201
	1	0.856 A @ 201-string	>201
	25	0.0113 A @ 201-string	>201

6.5. GFPD current during high-impedance blind spot ground faults

Based on the previous results, one may expect that the direction of the GFPD current could indicate blind spot ground faults, but this is not failsafe. Figure 40 (left) shows the GFPD current for 0.1, 0.25, and 0.5 A GFPD fuses for R_{fault}=25 Ω. In these simulations, there are two opposing currents through the GFPD: (1) the positive current from the array leakage, and (2) the negative current from the fault. For larger fault resistances, the current through the GFPD *does not* switch direction for larger arrays because the backfed fault current is smaller than the leakage current for large arrays. In other words, the leakage current per additional string is larger than the fault current per additional string. Figure 40 (right) shows this current contribution per string for module leakage and fault current as a function of fault resistance. For a 1 A GFPD with a 15 Ω or larger fault, the module leakage increases faster than fault current, so, for larger arrays, the GFPD current will not reverse direction.

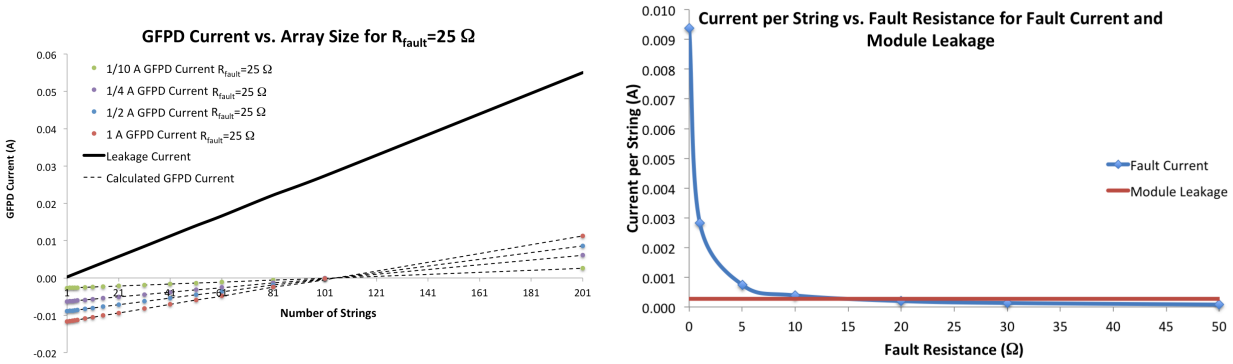

Figure 40: (left) Graph of GFPD current vs. array size for fault resistance of 25 Ω. The direction of the GFPD current will not change at an array size of 105 strings or larger, because for large R_{fault} values and large array sizes, the leakage current is larger than the fault current. (right) Graph of current per string as a function of fault resistance with I_{leak}=100 μA/module and RGFPD=0.252 Ω. For fault resistances of more than 15 Ω, the module leakage is larger than fault current, indicating that, as array size increases, the GFPD current will not reverse.

Figure 41 shows the circuit schematic for a 25 Ω fault resistance for array sizes of one, 101, and 201 strings. For a one-string array, the fault current is a hundred times larger than the leakage current. For a 101-string array, the leakage current and fault currents are approximately equal, so the GFPD current is nearly zero. For a 201-string array, the leakage current is larger than the fault current, and the GFPD current does not reverse direction.

These results indicate that for residential and smaller commercial-scale arrays, it would be possible to detect a blind spot fault by monitoring the direction of GFPD current. To determine the range of fault resistances that could be detected using this technique, simulations were performed for different array sizes varying R_{fault}. As fault resistance increases, the array size decreases for which there is a GFPD current reversal. Figure 42 shows the value of GFPD current vs. fault resistance for array sizes of eight, 21, 51, 101, and 201 strings with a 0.252 Ω (1 A) GFPD. The inset shows the crossover points. The fault resistance crossover point for larger array sizes is at a smaller R_{fault} due to the large amount of leakage current. For example, for an eight-string array, due to the smaller array size, the crossover would be at more than R_{fault}=110 Ω, but the 201-string array could only detect the blind spot using a change in GFPD current if the fault is less than about 20 Ω.

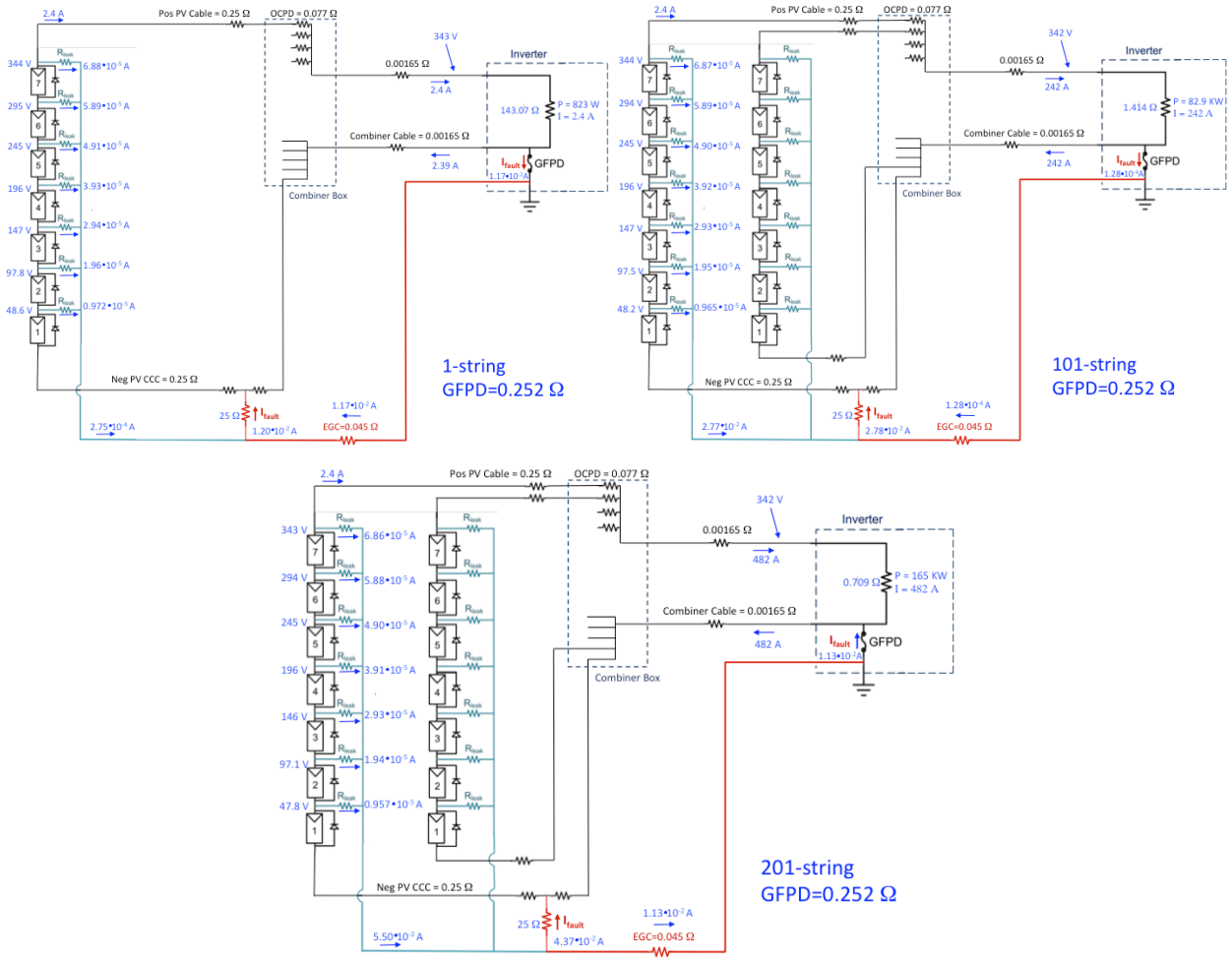

Figure 41: Three circuit schematics illustrating the reversal of GFPD current as array size increases. (top left) Circuit schematic of a one-string array with $I_{leak}<I_{fault}$ (top right), (bottom) 101-string array with $I_{leak}\approx I_{fault}$, and 201-string array with $I_{leak}>I_{fault}$.

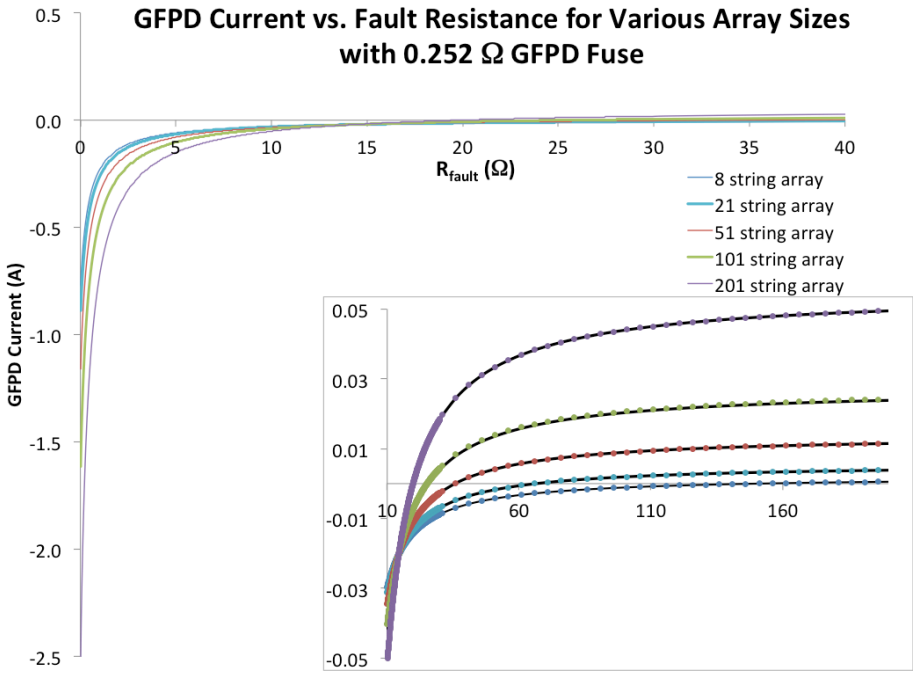

Figure 42: GFPD current as a function of fault resistance for various array sizes. The inset shows the crossover points for each array size.

6.6. Parametric study of GFPD current

As is apparent from Equation (27), the value of GFPD current is dependent on a number of parameters including number of strings (C), combiner cabling resistance (R_{comb}), resistance of the faulted section of PV cabling (R_x), GFPD resistance (R_{GFPD}), EGC resistance (R_{EGC}), and fault resistance (R_{fault}). In this section, a study of GFPD current is carried out by varying these system resistances across ranges denoted by Table 4. By determining how GFPD current varies with other parameters, it may be possible for system designers to decrease the blind spot window by maximizing GFPD current.

Table 4: Nominal and extreme values of the parametric resistance studies. A parametric analysis was completed for each parameter for the range of resistances listed below.

Parameter	*Nominal Value (Ω)*	*Low Value (Ω)*	*% Nominal*	*High Value (Ω)*	*% Nominal*
R_{fault}	--	0	--	10	--
R_{GFPD}	0.252	0.01	3.97	100	39,682
R_{EGC}	0.041	0.001	2.44	10	24,390
R_x	0.125 (40 ft)	0.002 (0.64 ft)	1.60	10 (3,200 ft)	8,000
R_{comb}	0.00165 (50 ft)	$1 \cdot 10^{-5}$ (0.30 ft)	0.61	0.3 (9,090 ft)	18,182

Figure 43 shows the results of the parametric analysis for GFPD current as a function of string number (upper left), and fault resistance (upper right), EGC resistance (lower left), and GFPD resistance (lower right) for a 101-string array. The blue line indicates the analytical solution

presented in Equation (27) while the black dots indicate the results of the SPICE simulation. The variables used in the simulation are listed in the corresponding graph. There is excellent correlation between the analytical equation and the SPICE simulations for this set of parametric analyses.

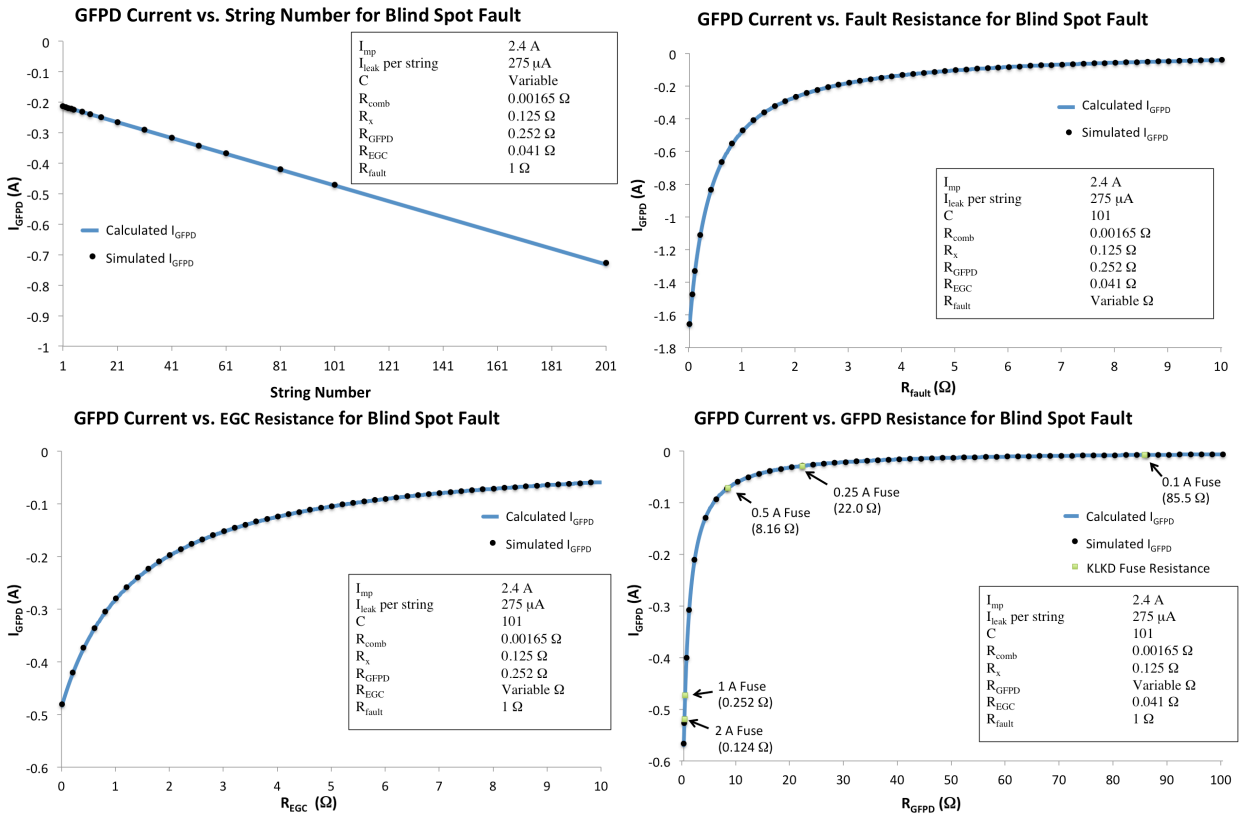

Figure 43: Comparison of analytical equation (blue trace) and SPICE simulations (black dots) for GFPD current as a function of other parasitic resistances. (upper left) GFPD current vs. number of strings in array. (upper right) GFPD current as a function of fault resistance. (lower left) GFPD current vs. EGC resistance. (lower right) GFPD current as a function of GFPD resistance. Green points indicate intrinsic resistance of KLKD "midget" fuses of various sizes from 0.1 to 2 A. For each graph, the variables used in the SPICE simulations are listed on each graph. In each set of simulations, the simulation results match well with the expected analytical solution.

Figure 44 (left) shows the parametric test results of GFPD current as a function of the faulted PV cabling resistance (R_x). For the PV cabling resistance, the SPICE simulations follow the analytical solution quite closely for small resistances. However, as the PV cabling resistance increases to values in the multiple ohm range, the simulation results are slightly smaller than expected. This is due to an assumption during the derivation of the analytical equation that each string stays at MPP. While this assumption is true for the majority of resistances, it may not hold true as the cabling resistance increases.

Figure 44 (right) shows the array voltage as a function of resistance changes. As the value of R_{fault}, R_{EGC}, and R_{GFPD} change, there is a small impact on the array voltage (less than 0.5 V), so the simulation and analytical results match well. The assumption that each string stays at MPP does not hold as well when R_x changes, so there is a larger effect on the array voltage (black dots and blue crosses). As the value of R_x approaches 10 Ω, the faulted string voltage changes by as much as 2 V. This small change in operation voltage is enough to cause the slight GFPD current mismatch between the simulation and analytical solutions.

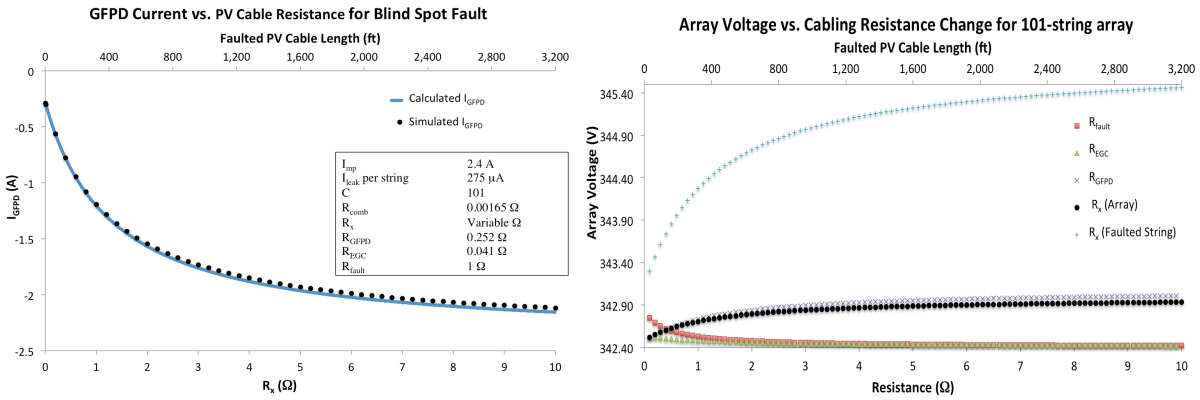

Figure 44: (left) GFPD current vs. PV cabling resistance of faulted string as determined through calculation of the analytical solution (blue trace) and SPICE simulations (black dots). The results match well for small resistances, but diverge slightly as R_x increases. This is due to the fact that as R_x increases, the operating voltage of the faulted string (right) can no longer be assumed to be at V_{mp} both before and after the fault.

The mismatch between simulation results and the analytical solution is similar for combiner cabling impedance changes (Figure 45). As the combiner cabling impedance increases to an appreciable fraction of the inverter impedance, the assumption that the array stays at MPP after the fault is no longer valid (Figure 45, right). This disruptive effect of the cabling impedance on the array voltage is much larger for large arrays because the inverter impedance is so low. This means even for small combiner cabling resistances, the array cannot be assumed to stay at MPP. Because smaller arrays have larger inverter impedances, the assumption holds for much larger cable impedances. As a result, the analytical solution is much closer to the simulation results as the array size decreases (Figure 46).

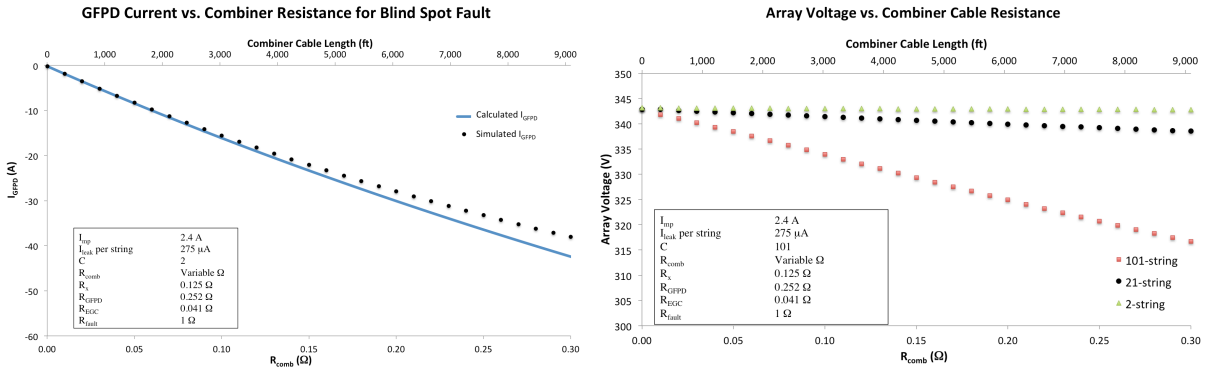

Figure 45: (left) GFPD current as a function of combiner cable resistance. The analytical calculation (blue trace) diverges from the SPICE simulation results as the resistance increases (black dots). This is due to the fact that as the cabling resistance becomes an appreciable function of inverter impedance, the array voltage can no longer be assumed to stay at MPP throughout the fault (right). The cabling impedance effect on array voltage is much larger for large arrays because the inverter impedance is so small.

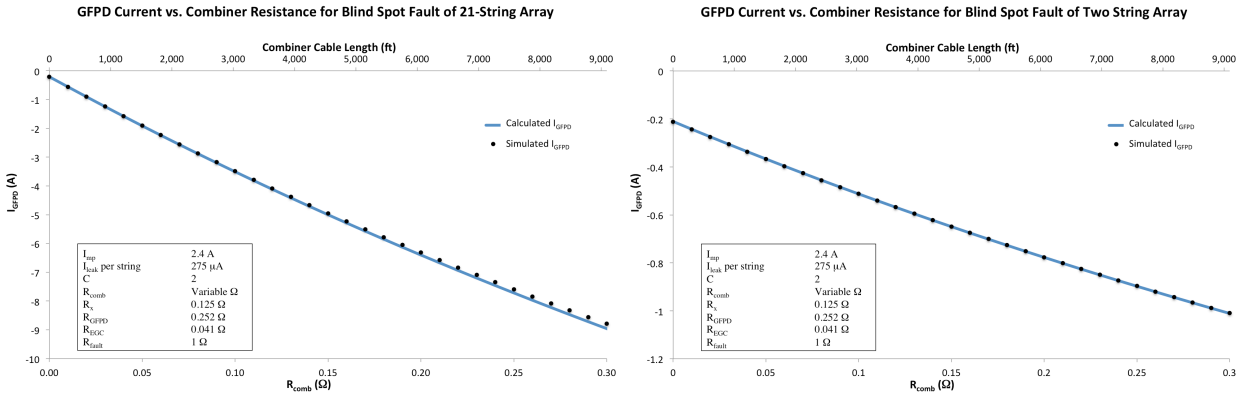

Figure 46: As the array size decreases, the analytical solution and SPICE simulation results begin to merge. While the mismatch is large for large array sizes, the mismatch is smaller as the array size goes to 21 strings (left) and is very close for a two-string array (right). The analytical and numerical results merge because, as inverter impedance increases, the PV cabling resistance has a much smaller effect on array voltage and the assumption that the array stays at V_{mp} is more accurate.

6.7. Blind spot ground fault conclusions

The results demonstrated the influence of fault and conductor resistances on the detectability of different blind spot ground faults. Blind spot detection is challenging due to the small GFPD current levels and the large influence of fault, GFPD, and cabling resistances on GFPD current. The SPICE model and analytical results were used to determine trends for various ground fault conditions and to ascertain potential benefits of reducing the fuse ratings in PV systems. Decreasing the GFPD ratings to 1 A for large installations would not increase the number of nuisance trips, but would protect against a wider range of ground faults. However, further decreasing the fuse ratings below 1 A does not improve the number of faults that can be detected

due to larger internal GFPD resistances and a subsequent decrease in fault current. In fact, because the ground fault fuse resistances increase from 1 A to 0.1 A, more blind spot faults can be detected with the 1 A fuse. Unfortunately, fewer ground faults to other parts of the array can be detected (IEC, 2005), so it is necessary to carefully select the GFPD rating to optimize the types of ground faults that can be detected.

While it may not be possible to provide complete detection for both faults within the array and faults to the grounded CCC using a fuse, the simulations indicate that the detection window for blind spot faults can be optimized by:

1) Minimizing leakage current, because fault current is the opposite direction of leakage current and large leakage currents will inhibit the detection of negative CCC faults;

2) Decreasing the fuse sizing for large arrays below UL 1741 requirements to 1 A, because module leakage current will remain too small to result in nuisance tripping and it will trip on more ground faults;

3) Preventing the reduction in fuses below 1 A because the internal resistance of the fuse prevents the fault current from passing through the GFPD;

4) Monitoring both GFPD current magnitude and direction (especially for smaller array sizes), because GFPD current can change direction when a negative CCC ground fault occurs; and

5) Employing other fault detection tools such as differential current measurement and insulation monitoring (see [13] for more information on alternative ground fault detection techniques and suggestions).

7. SUMMARY AND CONCLUSIONS

Many ground fault simulations were performed to determine if reducing the ground fault protection device (GFPD)—often called the ground fault detector/interrupter (GFDI)—fuse rating would increase the number and type of ground faults that could be detected without increasing the risk of nuisance tripping from leakage current. This work investigated the steady-state operation of PV arrays with different ground faults resistances at multiple locations. Ground fault simulations were carried out on arrays varying from two- to 201-string system with seven modules per string using both non-linear (arcing) and linear ground faults (solid connections). Ground faults were generated between each of the modules and the equipment grounding conductor.

Some of the findings from small system simulations include:

- Ground faults with resistances less than ~1000 Ω decreased array voltage, current, and power
- For a given value of R_{fault}, the fault and GFPD current increased nearly linearly as more modules of the string were faulted to ground.
- While modules in the unfaulted strings sourced greater current during a fault event, the applied voltage increased in the modules above the fault.
- If the value of R_{fault} was low enough and a significant number of modules are faulted, the applied voltage to these modules was equal to or greater than the module V_{oc}, the current in the faulted string reversed direction, and the unfaulted strings ended up backfeeding the fault.

To investigate nuisance tripping risks with decreased ground fault fuse ratings, simulations were carried out on two-, three-, and 10-string arrays with faults at multiple locations. Each module was simulated with various leakage currents from 1 μA through 1 mA. These simulations were used to find the maximum detectable fault resistance (R_{trip}^{max}) for fuses of 0.1 and 1 A. Some of the findings from these experimenters were:

- For leakage values consistent with IEC 61215 requirements, decreasing ground fault fuse ratings would drastically increase the number of detectable high-impedance ground faults while not increasing the risk of GFPD nuisance trips
- A 0.1 A fuse would detect ground fault resistances that are roughly 10x larger than a 1 A fuse
- At less than 100% irradiance levels, faults become even harder to detect because there is less current through the ground fault fuse. Low impedance faults are linear with the irradiance on the system, while high impedance faults are constant with respect to irradiance.

- The blind spot of modern GFPD systems are not limited to the grounded conductor—they can exist for ground faults from modules that are at a low potential
- The location of the fault is critical to the ability of the GFPD to detect it. Faults at 1+ are significantly more difficult to detect because the fault current through the GFPD is smaller than the other faults.
- Leakage currents for all arrays are small compared to the fault current.

As the size of the array increases, the effective resistance of the inverter to reach the maximum power point decreases. As a result, larger arrays are not more likely to detect high resistance ground faults. Larger arrays are, however, more likely to detect low resistance ground faults because the backfed current will be larger. This effect can be reduced, however as the GFPD rating is often increased from 1 to 5 A as the inverter size increases.

GFPD current was plotted for faults at various locations of one- through 201-string arrays with fault resistances of 0.01, 1, and 25 Ω. In order to protect an array from a 1+ fault, the fuse rating of a GFPD would have to be set at 1 A for a 0.01 Ω and 1 Ω fault. However, for a 25 Ω fault, the fuse rating would have to be decreased to 0.5 A.

Blind spot cases, where a fault occurs to the grounded current-carrying conductor, were simulated by including the internal resistance of the conductors and the GFPD. Surprisingly, decreasing the fuse ratings of PV installations does not improve the number of faults that can be detected. In fact, because the ground fault fuse resistances increase so drastically from 1 A to 0.1 A, more faults could be detected with the 1 A fuse. This is in contrast to the previous simulations of faults at 1+. In the case of blind spot faults, even though there is very little current through the GFPD it is often in the opposite direction of the leakage current and faults to different locations in the array, so it may be possible to detect ground faults by monitoring the voltage across the ground fault fuse.

Other simulations were performed to determine the influence of overcurrent protection in larger PV systems where the OCPD rating is equal to or less than the GFPD rating. Unfortunately, in these cases the OCPD clears, reducing the backfed current to zero, and the GFPD will no longer detect the fault.

In general, to detect the greatest number of ground faults in PV systems

- a low fuse rating (1 A and below) is needed for 1+ through 7+ faults, so long as it does not make the array susceptible to nuisance trips due to EMI noise and module leakage current
- a fuse with low internal resistance but high sensitivity (~1 A) is needed for blind spot ground faults in order for the fault current to pass through the GFPD

Based on these simulations, decreasing the GFPD ratings to 1 A for large systems would not increase the number of nuisance trips, but would protect against a wider range of ground faults. However, reducing the fuse ratings for residential and commercial sized arrays below 1 A is not advised because the detection sensitivity of blind spot faults is reduced.

Unfortunately, as shown in these simulations, GFPD fuses alone cannot detect all ground faults. Additional ground fault protections are recommended and discussed in detail in [13].

8. FUTURE WORK

The purpose of this work has been to demonstrate the use of SPICE in understanding blind spot faults in PV arrays. The data presented here is preliminary in nature and utilizes a simplistic model of a complicated system, e.g., excluding inverter maximum power point tracking, complex impedances, inverter bus capacitance, and AC feedback effects. While these computational simulations demonstrate a number of trends, they are no replacement for experimental data. (See the other Solar ABCs report on field measurements titled, "Final Report: Examination of Inverter Ground-Fault Detection 'Blind Spot' with Recommendations for Mitigation" for leakage and ground fault currents in real systems.) In order to truly calibrate the model to an actual PV system, it would be necessary to collect data from a real array and create controlled fault conditions. The generic PV system model was used to determine trends for various ground fault conditions and to ascertain potential benefits from reducing the fuse ratings in PV systems. By corroborating these findings with experimental results, recommendations for GFPD ratings changes to address current shortcomings in ground fault protection can be offered to assist the PV industry.

This page is intentionally left blank.

REFERENCES

[1] B. Brooks. (2012, Mar) Bakersfield Report *SolarPro*. 62-70.

[2] Y. Zhao, B. Lehman, J. de Palma, J. Mosesian, and R. Lyons, "Challenges to overcurrent protection devices under line-line faults in solar photovoltaic arrays," *Audio, Transactions of the IRE Professional Group on,* pp. 20-27, Sep 01 2011.

[3] L. W. Nagel and D. O. Pederson, "SPICE (Simulation Program with Integrated Circuit Emphasis)." vol. ERL-M382, ed: University of California, Berkeley, 1973, p. 62.

[4] L. Castaner and S. Silvestre, *Modelling Photovoltaic Systems using PSPICE*. Chichester, West Sussex, England: John Wiley and Sons Ltd, 2002.

[5] A. Devasia and S. K. Kurinec, "Teaching solar cell I-V characteristics using SPICE," *American Journal of Physics,* vol. 79 (12), p. 1232, 2011.

[6] J. Worden and M. Zuercher-Martinson. (2009, May) How Inverters Work. *SolarPro*. 68-85.

[7] J. Flicker, R. Kaplar, M. Marinella, and J. Granata, "PV Inverter Performance and Reliability: What is the Role of the Bus Capacitor?," *Photovoltaic Specialists Conference (PVSC)*, Austin, TX, 2012, p. 6.

[8] D. E. Collier and T. S. Key, "Electrical fault protection for a large photovoltaic power plant inverter," Photovoltaic Specialists Conference, 1988., Conference Record of the Twentieth IEEE, 1988.

[9] Y. Zhao, J. de Palma, J. Mosesian, R. Lyons, and B. Lehman, "Line-Line Fault Analysis and Protection Challenges in Solar Photovoltaic Arrays," 2009.

[10] Littelfuse, "POWR-GARD Fuse Datasheet," November 2011.

[11] W. B. Nottingham, "A New Equation for the Static Characteristic of the Normal Electric Arc," *American Institute of Electrical Engineers, Transactions of the,* vol. XIX pp. 302-310, Feb 01 1902.

[12] R. F. Ammerman, T. Gammon, P. K. Sen, and J. P. Nelson, "DC-Arc Models and Incident-Energy Calculations," *IEEE Transactions on Industry Applications,* vol. 46 (5), pp. 1810-1819.

[13] G. Ball, B. Brooks, J. Flicker, J. Johnson, A. Rosenthal, J. C. Wiles, and L. Sherwood, "Final Report: Examination of Inverter Ground-Fault Detection “Blind Spot” with Recommendations for Mitigation," Solar American Board for Codes and Standards, *In Press, 2013*.

[14] International Electrotechnical Commission, "Crystalline Silicon Terrestrial Photovoltaic (PV) Modules-Design Qualification and Type Approval," 2nd ed. Geneva, p. 102.

[15] Underwriters Laboratories, "Flat-Plate Photovoltaic Modules and Panels," 3rd ed. Northbrook, IL, 2008, pp. 1-82.

[16] J. A. del Cueto and T. J. McMahon, "Analysis of leakage currents in photovoltaic modules under high-voltage bias in the field," *Progress in Photovoltaics: Research and Applications,* vol. 10 (1), pp. 15-28, 2002.

[17] J. C. Wiles, "Photovoltaic System Grounding," ed, 2012, pp. 1-29.

[18] Underwriters' Laboratory, "Inverters, Converters, Controllers, and Interconnection System Equipment for Use with Distributed Energy Resources," UL 1741 ed. Northbrook, IL, 2001.

[19] Ferraz Shawmut, "HP6M(Amp Rating) Watts Loss Data," Ferraz Shawmut, Newburyport, MA2010.
[20] Socomec, "PV Fuses," General Catalog 2011-2012.
[21] Hill Technical Sales Group, "Solar PV Fuse," http://hilltech.com/products/power_components/Fuses/SolarPvFuseFusePhotovoltaicInverterPvCombinerFuse.html Accessed: 11/19/2012.
[22] SIBA Fuses, "URZ-DMI 10x38mm gR 1000 V Datasheet," Doc. Num. E19906, 2006.
[23] DF Electric, "Photovoltaic Fuse-links & Fuse Holders," 2012.
[24] Cooper-Bussmann, "Superior Protection for Solar Power Applications," Doc. Num. 3142, 2009.
[25] The ABB Group, "E 90 Range of Fuse Disconnectors and Fuseholders," 2010.
[26] B. Brooks, "The Ground-Fault Protection Blind Spot: Safety Concern for Larger PV Systems in the U.S.," Solar American Board for Codes and Standards, January 2012.

This page is intentionally left blank.

DISTRIBUTION

1	MS1033	Jay Johnson	06112
1	MS1033	Sigifredo Gonzalez	06112
1	MS1033	Jennifer E. Granata	06112
1	MS1033	Charles J. Hanley	06112
1	MS1084	Jack Flicker	01748
1	MS0899	Technical Library	09532 *(electronic copy)*


Sandia National Laboratories